Subspace-Based Near-Field Source Localization in Unknown Spatially Nonuniform Noise Environment

Weiliang Zuo ⓘ, *Member, IEEE*, Jingmin Xin ⓘ, *Senior Member, IEEE*, Nanning Zheng, *Fellow, IEEE*, Hiromitsu Ohmori, *Member, IEEE*, and Akira Sano, *Member, IEEE*

Abstract—In this paper, we investigate the problem of estimating the directions-of-arrival (DOAs) and ranges of multiple narrowband near-field sources in unknown spatially nonuniform noise (spatially inhomogeneous temporary white noise) environment, which is usually encountered in many practical applications of sensor array processing. A new subspace-based localization of near-field sources (SLONS) is proposed by exploiting the advantages of a symmetric uniform linear sensor array and using Toeplitzation of the array correlations. Firstly three Toeplitz correlation matrices are constructed by using the anti-diagonal elements of the array covariance matrix, where the nonuniform variances of additive noises are reduced to a uniform one, and then the location parameters (i.e., the DOAs and ranges) of near-field sources can be estimated by using the MUSIC-like method, while a new pair-matching scheme is developed to associate the estimated DOAs and ranges. Additionally, an alternating iterative scheme is considered to improve the estimation accuracy of the location parameters by utilizing the oblique projection operator, where the "saturation behavior" caused by finite number of snapshots is overcome effectively. Furthermore, the closed-form stochastic Cramér-Rao lower bound (CRB) is also derived explicitly for the near-field sources in the additive unknown nonuniform noises. Finally, the effectiveness of the proposed method and the theoretical analysis are substantiated through numerical examples.

Index Terms—Near-field, oblique projector, source localization, symmetric uniform linear array, unknown spatially nonuniform noises.

I. INTRODUCTION

LOCALIZATION of near-field sources is important in many practical application scenarios of sensor array processing

Weiliang Zuo, Jingmin Xin, and Nanning Zheng are with the Institute of Artificial Intelligence and Robotics, Xi'an 710049, China, and also with the National Engineering Laboratory for Visual Information Processing and Applications, Xi'an Jiaotong University, Xi'an 710049, China (e-mail: weiliang.zuo@xjtu.edu.cn; jxin@mail.xjtu.edu.cn; nnzheng@mail.xjtu.edu.cn).

Hiromitsu Ohmori and Akira Sano are with the Department of System Design Engineering, Keio University, Yokohama 223-8522, Japan (e-mail: ohm@sd.keio.ac.jp; sano@sd.keio.ac.jp).

such as sonar, collision avoidance radar, electronic surveillance, seismology, speech enhancement, and biomedical imaging (e.g., [1]–[13] and references therein), where the near-field source is characterized by two independent location parameters (i.e., the directions-of-arrival (DOAs) and the ranges), and the correct pair-matching (i.e., association) of the estimated DOAs and ranges is required, while the far-field source is only parameterized by the DOA. In past decades, the localization of near-field sources was extensively studied (e.g., [14]–[34]). Among them, many maximum likelihood methods and subspace-based methods were proposed by using the second-order statistics (SOS) for spatially and temporally white Gaussian noises with the uniform variance or arbitrary noises with known statistics [14]–[32], while some subspace-based methods were presented by using the higher-order statistics (HOS) for spatially and temporally white or colored Gaussian noises [33], [34]. However, the homogeneous noise assumption is often invalid and the noise covariance matrix is usually unavailable in some applications (see, e.g., [35]–[42], [105]–[107]), which causes most subspace-based methods for the far-field sources (see, e.g., [43]–[47], [108]–[114]) to be severely degraded, and hence a variety of DOA estimation methods were developed for the far-field sources in the unknown colored noise [48]–[55] or unknown nonuniform noises [56]–[75]. Similarly in the presence of unknown nonuniform noises, most of the aforementioned SOS-based localization methods for the near-field sources will seriously deteriorate [14]–[32], while the HOS-based localization methods [33], [34] only apply to the non-Gaussian near-field sources. To the best of our knowledge, the localization of near-field sources in unknown spatially nonuniform noise environment has not been well studied in the literature of array processing. By using the multiple signal classification (MUSIC) [44], the two-dimensional (2D) MUSIC-whitened noise (MUSIC-WN) and the 2D MUSIC-smooth sparse arrays (MUSIC-SSA) were suggested in [76], where the noise-only array data or well-separated subarrays is required to whiten or eliminate the effect of additive noises, but a signal-free environment is not always available in practice and this requirement may restrict the practical applications (cf. [60], [54]). In addition, the far-field sources and the near-field sources usually coexist (see, e.g., [28] and references therein for details), and recently some HOS-based methods were proposed to localize the far-field and near-field sources in the presence of the additive white or colored Gaussian noises [77]–[84].

Therefore, in this paper, we deal with the localization of multiple near-field sources impinging on the symmetric uniform linear sensor array in the unknown spatially additive nonuniform noises (spatially inhomogeneous temporary white Gaussian noises), where the estimated DOAs should be associated with the corresponding estimated ranges of the same source. Based on our preliminary study [85], a new subspace-based localization of near-field sources (SLONS) is proposed by using the anti-diagonal correlation elements of the array covariance matrix, which can be interpreted as the received "signals" for a virtual ULA and contain only one noise variance or no noise variance. First by constructing two Toeplitz correlation matrices with the correlation elements along the major anti-diagonal or that along the 2nd upper diagonal off the major anti-diagonal of the array covariance matrix to eliminate the effects of unknown additive nonuniform noises, two auxiliary parameters related to the DOAs and ranges of near-field sources can be estimated separately from these two resulting matrices by using the MUSIC-like method [44]. As a result, we can obtain two sets of the estimated electric angles, which are functions of the location parameters (i.e., the DOAs and ranges). Then by forming another Toeplitz correlation matrix with the correlation elements along the 1st upper diagonal off the major anti-diagonal of the array covariance matrix, a pair-matching scheme is developed to associate two sets of the estimated electric angles by searching for the minimum value of the cost function, which is formed with the noise subspace of the resulting Toeplitz matrix, and consequently the estimated DOA and range of the same source can be obtained. Obviously unlike the pairing scheme presented in [23] for the near-field sources, which requires some constraints on the electric angles of sources, this new pair-matching scheme can applied to more general sources. Additionally an alternating iterative scheme is presented to improve the estimation accuracy of the location parameters by utilizing the oblique projection operator [86], where the "saturation behavior" (i.e., the estimated DOAs and ranges may have high elevated error floors, which do not decrease with the increasing signal-to-noise ratio (SNR)) caused by finite number of snapshots is overcome effectively. Furthermore, the stochastic Cramér-Rao lower bound (CRB) for the near-field sources in unknown nonuniform noises is derived explicitly. Finally, the effectiveness of the proposed method and the theoretical analysis are verified through numerical examples, and simulation results show that the proposed method achieves a remarkable estimation performance. Compared with the previous conference paper [85], the detailed theoretical derivation of the CRB is presented for the near-field sources in the unknown nonuniform noises, and the computational complexity of the proposed SLONS is also analyzed.

Glossary of Notation: The following notations are used through this paper. $\boldsymbol{I}_m$, $\boldsymbol{O}_{m \times n}$, $\boldsymbol{0}_{m \times 1}$, and $\delta_{n,t}$ stand for the $m \times m$ identity matrix, the $m \times n$ null matrix, the $m \times 1$ null vector, and the Kronecker delta, $\boldsymbol{e}_l$, $\bar{\boldsymbol{e}}_l$, and $\tilde{\boldsymbol{e}}_l$, stand for the $(M+1) \times 1$, $M \times 1$, and $(2M+1) \times 1$ unit vector with a unity element at the lth, lth, and $(M+1+l)$th location and zeros elsewhere, and $E\{\cdot\}$, $\{\cdot\}^*$, $(\cdot)^T$, and $(\cdot)^H$ represent the statistical expectation, the complex conjugate, the transposition, and the Hermitian transposition, respectively. Additionally,
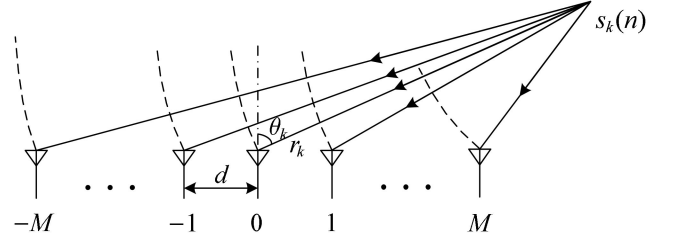

Fig. 1. The localization of near-field sources with a symmetric uniform linear sensor array.

$\mathrm{diag}(\cdot)$, $\mathrm{tr}\{\cdot\}$, $\mathrm{rank}\{\cdot\}$, and $\mathcal{R}(\cdot)$ denote the diagonal matrix operator, the trace operator, the rank and the range space of the bracketed matrix, respectively, while $\otimes$, $\odot$, and $\oplus$ signify the Kronecker product, the Hadamard-Schur product, and the direct sum operator. Furthermore $\mathrm{vec}(\cdot)$ is a matrix operation to stack the columns of the bracketed matrix one under the other beginning with the leftmost column, $\mathcal{O}[\cdot]$ indicates the order of magnitude, $\mathrm{span}\{\cdot\}$ denotes the columns space spanned by the column vectors of the bracketed matrix, and $\hat{x}$ means the estimate of x.

II. DATA MODEL AND ASSUMPTIONS

As depicted in Fig. 1, we consider a symmetric uniform linear sensor array consisting of $2M + 1$ sensors and K narrowband noncoherent signals $\{s_k(n)\}$ impinging on this array from the near-field sources with the unknown location parameters $\{\theta_k, r_k\}$, where θ_k is the DOA of the source signal $s_k(n)$ measured at the reference sensor relative to the normal of array, r_k is the corresponding range between the signal source and the reference sensor and given by $r_k \in (0.62(D^3/\lambda)^{1/2}, 2D^2/\lambda)$ [14], while D is the aperture of array given by $D = 2Md$ herein (cf. [4]), d is the sensor spacing, and λ is the wavelength. The received noisy signal $x_m(n)$ at the mth sensor can be approximated as

$$x_m(n) = \sum_{k=1}^{K} s_k(n) e^{j\tau_{mk}} + w_m(n) \tag{1}$$

for $m = -M, \ldots, -1, 0, 1, \ldots, M$, where $w_m(n)$ is the additive noise, and τ_{mk} is the phase delay due to the time delay between the reference sensor and the mth sensor for the signal $s_k(n)$ from the kth near-field source, which is given by (cf. [14])

$$\tau_{mk} = \frac{2\pi}{\lambda} \left(\sqrt{r_k^2 + (md)^2 - 2\,mdr_k \sin\theta_k} - r_k \right). \tag{2}$$

Further, τ_{mk} in (2) can be approximated with the second-order Taylor expansion as [14], [23]

$$\tau_{mk} \approx m\psi_k + m^2\phi_k \tag{3}$$

where ψ_k and ϕ_k are called as the electric angles (include the DOAs and ranges) defined by

$$\psi_k \triangleq -\frac{2\pi d}{\lambda} \sin\theta_k \tag{4}$$

$$\phi_k \triangleq \frac{\pi d^2}{\lambda r_k} \cos^2 \theta_k. \tag{5}$$

Then the received data $\{x_m(n)\}$ can be rewritten compactly by using vector-matrix notation as

$$\boldsymbol{x}(n) = \boldsymbol{A}\boldsymbol{s}(n) + \boldsymbol{w}(n) \tag{6}$$

where $\boldsymbol{x}(n)$, $\boldsymbol{s}(n)$, and $\boldsymbol{w}(n)$ are the vectors of the received data, the incident signals and the additive noises given by $\boldsymbol{x}(n) \triangleq [x_{-M}(n), \ldots, x_{-1}(n), x_0(n), x_1(n), \ldots, x_M(n)]^T$, $\boldsymbol{s}(n) \triangleq [s_1(n), s_2(n), \ldots, s_K(n)]^T$, and $\boldsymbol{w}(n) \triangleq [w_{-M}(n), \ldots, w_{-1}(n), w_0(n), w_1(n), \ldots, w_M(n)]^T$, while $\boldsymbol{A}$ is the array response matrix defined by $\boldsymbol{A} \triangleq [\boldsymbol{a}(\theta_1, r_1), \boldsymbol{a}(\theta_2, r_2), \ldots, \boldsymbol{a}(\theta_K, r_K)]$, and $\boldsymbol{a}(\theta_k, r_k)$ is the array steering vectors which can be expressed as $\boldsymbol{a}(\theta_k, r_k) \triangleq [e^{-jM\psi_k}e^{jM^2\phi_k}, \ldots, e^{-j\psi_k}e^{j\phi_k}, 1, e^{j\psi_k}e^{j\phi_k}, \ldots, e^{jM\psi_k}e^{jM^2\phi_k}]^T$.

Here we make the basic assumptions as follows.

A1) The array is calibrated and the array response matrix $\boldsymbol{A}$ has full rank and is unambiguous.

A2) Without loss of generality, the incident signals $\{s_k(n)\}$ from the K near-field sources are temporally complex white Gaussian random processes with zero-mean and the variance given by $E\{s_k(n)s_k^*(t)\} = r_{s_k}\delta_{n,t}$ and $E\{s_k(n)s_k(t)\} = 0, \forall n, t$.

A3) For the simplicity of theoretical performance analysis, the additive noises $\{w_i(n)\}$ are temporally and spatially complex Gaussian random processes with zero-mean, and the covariance matrix of unknown additive noises is given by

$$\boldsymbol{Q} \triangleq E\{\boldsymbol{w}(n)\boldsymbol{w}^H(n)\}$$
$$= \text{diag}(\sigma_{-M}^2, \ldots, \sigma_{-1}^2, \sigma_0^2, \sigma_1^2, \ldots, \sigma_M^2) \tag{7}$$

where σ_m^2 is the noise power at the mth sensor. Moreover, the covariance matrices $E\{\boldsymbol{w}(n)\boldsymbol{w}^T(t)\} = \boldsymbol{O}_{(2M+1)\times(2M+1)}$, $\forall n, t$. Additionally the additive noises $\{w_m(n)\}$ are independent to the incident signals $\{s_k(n)\}$, i.e., $E\{\boldsymbol{s}(n)\boldsymbol{w}^H(n)\} = E\{\boldsymbol{s}(n)\boldsymbol{w}^T(n)\} = \boldsymbol{O}_{K\times(2M+1)}$.

A4) The number of near-field sources K is known, and K satisfies the relation $K < M$ (cf. Remark C for details).

A5) The sensor spacing d satisfies the relation $d \leq \lambda/4$ for avoiding the estimation ambiguity.

In the following, we concentrate on the estimation of location parameters $\{\theta_k\}_{k=1}^K$ and $\{r_k\}_{k=1}^K$ of multiple near-field sources from the finite noisy array data $\{\boldsymbol{x}(n)\}_{n=1}^N$, where the basic idea is firstly to transfer the nonuniform noise into an uniform one and then to estimate the location parameters from the reformed data model under the virtual uniform noise environment.

Remark A: Various localization techniques have been developed in many application fields (see [6], [7] and references therein), where the time-of-arrival (TOA), the time-difference-of-arrival (TDOA), the received signal strength (RSS), and the DOA are commonly used measurements for source localization (e.g., [87]–[90]). Basically the TOA, TDOA, and RSS provide the distance information between the source and the sensors, while the DOA gives the source bearing relative to the sensors. Perhaps the TDOA is the most widely used technique for passive

localization [90], it measures the difference in time between the source signal received by a pair of spatially separated sensors (i.e., two receivers), where the sensors are required to be synchronized to a common time reference. By multiplying the TDOA with a known propagation speed, the range difference between the source and two sensors can be obtained. As a result, the source location is given by the intersection of at least two hyperbolas, where a hyperbola is defined by the range difference between the source and two sensors. Obviously it will be rather difficult and complicated to localize multiple sources by using the TDOA technique, though the TDOA localization was studied for one source in far-field and near-field [89]. In this paper, we consider the localization of multiple near-field source by estimating their DOAs and ranges. □

III. NEW SUBSPACE-BASED LOCALIZATION OF NEAR-FIELD SOURCES–SLONS

Here we develop a method called SLONS for estimating the DOAs and ranges of multiple near-field sources by exploiting the special configuration of a symmetric uniform linear array. The proposed SLONS includes three stages: 1) estimate the location parameters (i.e., DOAs and ranges) of the near-fields sources, 2) associate the estimated DOAs and ranges, and 3) performance improvement against finite snapshots.

A. Direction-of-Arrival Estimation of Near-Field Sources

From (6), we obtain the array covariance matrix $\boldsymbol{R}$ as

$$\boldsymbol{R} \triangleq E\{\boldsymbol{x}(n)\boldsymbol{x}^H(n)\} = \boldsymbol{A}\boldsymbol{R}_s\boldsymbol{A}^H + \boldsymbol{Q} \tag{8}$$

where $\boldsymbol{R}_s \triangleq E\{\boldsymbol{s}(n)\boldsymbol{s}^H(n)\} = \text{diag}(r_{s_1}, r_{s_2}, \ldots, r_{s_K})$ with $r_{s_k} \triangleq E\{s_k(n)s_k^*(n)\}$, and the anti-diagonal correlation element of $\boldsymbol{R}$ is given by (cf. [23])

$$R_i(p) \triangleq E\{x_p(n)x_{-p-i}^*(n)\}$$
$$= \boldsymbol{r}_{is}^T\boldsymbol{b}_i(p) + \sigma_{0.5i}^2\delta_{p,-p-i} \tag{9}$$

for $i = -2M, \ldots, -1, 0, 1, \ldots, 2M$ and $p = -M + i_2, \ldots, -1, 0, 1, \ldots, M - i_1$, where $i_1 = 0.5(|i| + i)$, $i_2 = 0.5(|i| - i)$, $\boldsymbol{b}_i(p) \triangleq [e^{j2p\gamma_{i1}}, e^{j2p\gamma_{i2}}, \ldots, e^{j2p\gamma_{iK}}]^T$, $\boldsymbol{r}_{is} \triangleq [r_{s_1}e^{ji\gamma_{i1}}, r_{s_2}e^{ji\gamma_{i2}}, \ldots, r_{s_K}e^{ji\gamma_{iK}}]^T$, $\gamma_{ik} = \psi_k - i\phi_k$, and $\sigma_{0.5i}^2 = 0$ when i is odd. Herein we easily have

$$\psi_k = \gamma_{0k} \tag{10}$$

$$\phi_k = \frac{1}{2}(\gamma_{0k} - \gamma_{2k}). \tag{11}$$

Obviously $\{R_i(p)\}$ can be interpreted as the received "signals" for a virtual array of $2M + 1 - |i|$ sensors illuminated by K "signals" $\{r_{s_k}e^{ji\gamma_{ik}}\}$, and $\{R_i(p)\}$ differ only by a phase factor γ_{ik}. Hence the auxiliary parameter γ_{ik} can be estimated by using the phase delays of $\{R_i(p)\}$.

By setting $i = 0$ (i.e., $i_1 = i_2 = 0$), we have $p = -M, -M + 1, \ldots, -1, 0, 1, \ldots, M - 1, M$. Therefore, by using the $2M + 1$ correlations $\{R_0(p)\}_{p=-M}^M$ along the major cross-diagonal of $\boldsymbol{R}$ (i.e., $i = 0$), we can form an $(M+1) \times (M+1)$ Toeplitz

matrix T_0 as

$$T_0 = \begin{bmatrix} R_0(0), & R_0(-1), & \cdots, & R_0(-M) \\ R_0(1), & R_0(0), & \cdots, & R_0(-M+1) \\ \vdots & \vdots & \ddots & \vdots \\ R_0(M), & R_0(M-1), & \ldots, & R_0(0) \end{bmatrix} \quad (12)$$

where its (l,t)th element can be represented as

$$(T_0)_{l,t} = R_0(l-t) \quad (13)$$

for $l, t = 1, 2, \ldots, M+1$, in which the tth column c_{0t} of T_0 is given by

$$c_{0t} \triangleq [(T_0)_{1,t}, (T_0)_{2,t}, \ldots, (T_0)_{M+1,t}]^T. \quad (14)$$

By substituting (9) into (14), after some simple manipulations, we have

$$\begin{aligned} c_{0t} &= [R_0(1-t), R_0(2-t), \ldots, R_0(M+1-t)]^T \\ &= [b_0(1-t), b_0(2-t), \ldots, b_0(M+1-t)]^T r_{0s} \\ &\quad + [0_{(t-1)\times 1}^T, \sigma_0^2, 0_{(M+1-t)\times 1}^T]^T \\ &= A_0 D_0^{1-t} r_{0s} + \sigma_0^2 e_t \end{aligned} \quad (15)$$

where the Kronecker delta $\delta_{l-t,-l+t} = 1$ for $l-t = -l+t$ (i.e., $l = t$) is used, and $D_0 = \text{diag}(e^{j2\gamma_{01}}, e^{j2\gamma_{02}}, \ldots, e^{j2\gamma_{0K}})$, while $A_0 \triangleq [b_0(0), b_0(1), \ldots, b_0(M)]^T$ with the dimension $(M+1) \times K$. Then from (13)–(15), the Teoplitz correlation matrix T_0 in (12) can be rewritten as

$$\begin{aligned} T_0 &= [c_{01}, c_{02}, \ldots, c_{0,M+1}] \\ &= A_0 [R_s b_0(0), R_s b_0^*(1), \ldots, R_s b_0^*(M)] + \sigma_0^2 I_{M+1} \\ &= A_0 R_s A_0^H + \sigma_0^2 I_{M+1}. \end{aligned} \quad (16)$$

Clearly the nonuniform noise matrix Q in (8) is transformed to a uniform one $\sigma_0^2 I_{M+1}$ in (16), and we can see that the matrix A_0 is a Vandermonde matrix with full rank, while the eigenvalue decomposition (EVD) of the matrix T_0 in (16) is given by

$$T_0 = U_{0s} \Lambda_{0s} U_{0s}^H + U_{0n} \Lambda_{0n} U_{0n}^H \quad (17)$$

where Λ_{0s} and Λ_{0n} are the diagonal matrices consisting of the K largest and the $M+1-K$ smallest eigenvalues respectively, while the $(M+1) \times K$ signal subspace matrix U_{0s} and the $(M+1) \times (M+1-K)$ noise subspace matrix U_{0n} consist of the corresponding eigenvectors, respectively. The columns of the Vandermonde matrix A_0 and the columns of the signal subspace matrix U_{0s} span the same subspace, i.e., $\text{span}\{A_0\} = \text{span}\{U_{0s}\}$. As a result, we have

$$U_{0n}^H A_0 = O_{(M+1)\times K}. \quad (18)$$

Therefore by using the relation (18), we can easily get the estimates of the auxiliary parameters $\{\gamma_{0k}\}_{k=1}^K$ (i.e., the DOAs $\{\theta_k\}_{k=1}^K$) with the conventional MUSIC method [44]. Furthermore, when the number of snapshots is finite, the auxiliary parameters $\{\gamma_{0k}\}_{k=1}^K$ can be estimated by minimizing the following MUSIC-like cost function (cf. [44])

$$f_0(\gamma_{0k}) = a_0^H(\gamma_{0k}) \hat{U}_{0n} \hat{U}_{0n}^H a_0(\gamma_{0k}) \quad (19)$$

where $a_0(\gamma_{0k})$ denotes the kth column of A_0 given by $a_0(\gamma_{0k}) = [1, e^{j2\gamma_{0k}}, \ldots, e^{j2M\gamma_{0k}}]^T$. Then from (4) and (10), we can find that the DOAs of the near-field sources can be estimate from the auxiliary parameter $\{\gamma_{0k}\}_{k=1}^K$ (see details in Section III-C).

B. Range Estimation of Near-Field Sources

Similarly by setting $i = 2$ (i.e., $i_1 = 2, i_2 = 0$, and $p = -M, -M+1, \ldots, -1, 0, 1, \ldots, M-3, M-2$) and by using the $2M-1$ correlations $\{R_2(p)\}_{p=-M}^{M-2}$ along the 2nd upper diagonal off the major cross-diagonal of R, we can form another $M \times M$ Toeplitz matrix T_2 as

$$\begin{aligned} T_2 &= \begin{bmatrix} R_2(-1), & R_2(-2), & \cdots, & R_2(-M) \\ R_2(0), & R_2(-1), & \cdots, & R_2(-M+1) \\ \vdots & \vdots & \ddots & \vdots \\ R_2(M-2), & R_2(M-3), & \cdots, & R_2(-1) \end{bmatrix} \\ &= A_2 R_s A_2^H + \sigma_M^2 I_M \end{aligned} \quad (20)$$

where the (l,t)th element of T_2 can be represented as

$$(T_2)_{l,t} = R_2(l-t-1) \quad (21)$$

for $l, t = 1, 2, \ldots, M$, and $A_2 \triangleq [b_2(0), b_2(1), \ldots, b_2(M-1)]^T$. Obviously the nonuniform noise matrix Q in (8) is transformed to a uniform one $\sigma_1^2 I_M$ in (20), and the matrix A_2 is a Vandermonde matrix, which has full rank. Hence the EVD of the matrix T_2 in (20) is given by

$$T_2 = U_{2s} \Lambda_{2s} U_{2s}^H + U_{2n} \Lambda_{2n} U_{2n}^H \quad (22)$$

where Λ_{2s} and Λ_{2n} are the diagonal matrices consisting of the K largest and the $M-K$ smallest eigenvalues respectively, while the $M \times K$ signal subspace matrix U_{2s} and the $M \times (M-K)$ noise subspace matrix U_{2n} consists of the corresponding eigenvectors, respectively. Then we easily have

$$U_{2n}^H A_2 = O_{M \times K}. \quad (23)$$

When the number of snapshots is finite, the auxiliary parameters $\{\gamma_{2k}\}_{k=1}^K$ can be estimated by minimizing the following MUSIC-like cost function (cf. [44])

$$f_2(\gamma_{2k}) = a_2^H(\gamma_{2k}) \hat{U}_{2n} \hat{U}_{2n}^H a_2(\gamma_{2k}) \quad (24)$$

where $a_2(\gamma_{2k})$ denotes the kth column of A_2 given by $a_2(\gamma_{2k}) = [1, e^{j2\gamma_{2k}}, \ldots, e^{j2M\gamma_{2k}}]^T$.

Although two sets of the auxiliary parameters $\{\hat{\gamma}_{0k}\}_{k=1}^K$ and $\{\hat{\gamma}_{2k}\}_{k=1}^K$ are estimated separately with (19) and (24), there is no clear one-to-one relationship between each element of these two estimation sets. From (10) and (11), we easily get K estimates $\{\hat{\psi}_1, \hat{\psi}_2, \ldots, \hat{\psi}_K\}$ of the electric angle ψ_k (a function of DOA θ_k as shown in (4)) and K^2 temporary estimates $\{\hat{\phi}_{11}, \hat{\phi}_{12}, \ldots, \hat{\phi}_{1K}, \ldots, \hat{\phi}_{KK}\}$ of the electric angle ϕ_k (which is a function of DOA θ_k and range r_k) by

$$\hat{\psi}_k = \hat{\gamma}_{0k}, \quad \hat{\phi}_{kk'} = 0.5(\hat{\gamma}_{0k} - \hat{\gamma}_{2k'}) \quad (25)$$

for $k = 1, 2, \ldots, K$ and $k' = 1, 2, \ldots, K$. In order to estimate and associate the DOA and range of the same near-field source from these two separate sets of estimates $\{\hat{\psi}_k\}_{k=1}^K$ and

$\{\hat{\phi}_{kk'}\}_{k,k'=1}^K$, an additional procedure of pair-matching is required.

C. Parameter Pairing and Estimation of DOA and Range

Although two sets of the estimated electric angles $\hat{\psi}_k$ and $\hat{\phi}_{kk'}$ are obtained in (25) for $k = 1, 2, \ldots, K$ and $k' = 1, 2, \cdots, K$, they should be associated with a corresponding source to estimate the location parameters (i.e., the DOA and range) of the same near-field source. Now we consider a new pair-matching scheme for the DOA and range estimation.

Herein by setting $i = 1$ (i.e., $i_1 = 1, i_2 = 0, p = -M, -M + 1, \ldots, -1, 0, 1, \ldots, M - 2, M - 1$) and by employing the $2M - 1$ correlations $\{R_1(p)\}_{p=-M+1}^{M-1}$ along the 1st upper diagonal off the major cross-diagonal of $\boldsymbol{R}$ in (9), we can form a new $M \times M$ Toeplitz matrix $\boldsymbol{T}_1$ as

$$
\boldsymbol{T}_1 = \begin{bmatrix} R_1(0), & R_1(-1), & \cdots, R_1(-M+1) \\ R_1(1), & R_1(0), & \cdots, R_1(-M+2) \\ \vdots & \vdots & \ddots & \vdots \\ R_1(M-1), R_1(M-2), \cdots, & R_1(0) \end{bmatrix}
$$
$$
= \boldsymbol{A}_1 \bar{\boldsymbol{R}}_s \boldsymbol{A}_1^H \tag{26}
$$

where the (l, t)th element of $\boldsymbol{T}_1$ can be represented as

$$
(\boldsymbol{T}_1)_{l,t} = R_1(l - t) \tag{27}
$$

for $l, t = 1, 2, \ldots, M$, $\boldsymbol{A}_1 \triangleq [\boldsymbol{b}_1(0), \boldsymbol{b}_1(1), \ldots, \boldsymbol{b}_1(M - 1)]^T$, and $\bar{\boldsymbol{R}}_s = \mathrm{diag}(r_{s_1} e^{ji\gamma_{i1}}, r_{s_2} e^{ji\gamma_{i2}}, \ldots, r_{s_K} e^{ji\gamma_{iK}})$. Then the EVD of the matrix $\boldsymbol{T}_1$ is given by

$$
\boldsymbol{T}_1 = \boldsymbol{U}_{1s} \boldsymbol{\Lambda}_{1s} \boldsymbol{U}_{1s}^H + \boldsymbol{U}_{1n} \boldsymbol{\Lambda}_{1n} \boldsymbol{U}_{1n}^H \tag{28}
$$

where $\boldsymbol{\Lambda}_{1s}$ and $\boldsymbol{\Lambda}_{1n}$ are the diagonal matrices consisting of the K largest eigenvalues (i.e., nonzero) and the $M - K$ smallest eigenvalues (i.e., zeros) respectively, while $\boldsymbol{U}_{1s}$ and $\boldsymbol{U}_{1n}$ are the $M \times K$ signal subspace and the $M \times (M - K)$ noise subspace, respectively. When the number of snapshots is finite, we can estimate $\{\gamma_{1k}\}_{k=1}^K$ by minimizing the following cost function

$$
f_1(\gamma_{1k}) = \boldsymbol{a}_1^H(\gamma_{1k}) \hat{\boldsymbol{U}}_{1n} \hat{\boldsymbol{U}}_{1n}^H \boldsymbol{a}_1(\gamma_{1k}) \tag{29}
$$

where $\boldsymbol{a}_{1k}(\gamma_{1k})$ denotes the kth column of $\boldsymbol{A}_1$ given by $\boldsymbol{a}_1(\gamma_{1k}) = [1, e^{j2\gamma_{1k}}, \ldots, e^{j2M\gamma_{1k}}]^T$. Hence from (25) and (29), the estimated electric phase angles $\hat{\psi}_{k_o}$ and $\hat{\phi}_{kk'_o}$ can be associated with the indices (k_o, k'_o) determined by

$$
(k_o, k'_o) = \arg \min_{(k,k')} f_1(\hat{\psi}_k, \hat{\phi}_{kk'}) \tag{30}
$$

for $k, k' = 1, 2, \ldots, K$.

Finally by using these paired estimates $\hat{\psi}_{k_o}$ and $\hat{\phi}_{k_o,k'_o}$ (i.e., $\hat{\psi}_k$ and $\hat{\phi}_k$), from (4) and (5), the DOA θ_k and range r_k of the incident signal $s_k(n)$ are obtained as

$$
\hat{\theta}_k = \arcsin(\alpha_1 \hat{\psi}_k) \tag{31}
$$
$$
\hat{r}_k = \frac{\alpha_2}{\hat{\phi}_k} \cos^2(\hat{\theta}_k) = \frac{\alpha_2}{\hat{\phi}_k} \cos^2(\arcsin(\alpha_1 \hat{\psi}_k)) \tag{32}
$$

where $\alpha_1 = -\lambda/(2\pi d)$, and $\alpha_2 = \pi d^2/\lambda$. As a result, the location parameters (i.e., $\{\hat{\theta}_k, \hat{r}_k\}_{k=1}^K$) of the same near-field source can be estimated.

D. Alternating Iterative Scheme Against Finite Snapshots

When the number of snapshots is not sufficiently large enough, the nonzero residual cross-correlations between the incident signals will cause the estimated matrices $\hat{\boldsymbol{R}}_s$ and $\hat{\boldsymbol{R}}$ (and hence the Toeplitz matrices $\hat{\boldsymbol{T}}_0, \hat{\boldsymbol{T}}_1$, and $\hat{\boldsymbol{T}}_2$) be inaccurate. Consequently the estimated DOA $\hat{\theta}_k$ and range $\hat{r}_k$ may have high elevated error floors, which do not decrease with the increasing SNR (i.e., "saturation behavior") (cf. [91]–[93]). Since the range space of each incident signal is nonoverlapping and not orthogonal to that of the others, we can use the oblique projection operator [86] to isolate one signal from the others and present an alternating iterative scheme to improve the performance with finite snapshots of array data.

By defining $\boldsymbol{a}_k \triangleq \boldsymbol{a}(\theta_k, r_k)$ and denoting the reduced signal vector without $s_k(n)$ and the corresponding reduced array response matrix without column $\boldsymbol{a}_k$ as $\bar{\boldsymbol{s}}_k(n)$ and $\bar{\boldsymbol{A}}_k$, where $\mathcal{R}(\boldsymbol{A}) = \mathcal{R}(\boldsymbol{a}_k) \oplus \mathcal{R}(\bar{\boldsymbol{A}}_k)$, we can obtain

$$
\hat{\boldsymbol{R}}_s = \begin{bmatrix} \hat{r}_{s_k}, & \hat{\boldsymbol{\rho}}^T \\ \hat{\boldsymbol{\rho}}^*, & \hat{\bar{\boldsymbol{R}}}_k \end{bmatrix} \tag{33}
$$
$$
\hat{\boldsymbol{R}} = \hat{r}_{s_k} \boldsymbol{a}_k \boldsymbol{a}_k^H + \boldsymbol{a}_k \hat{\boldsymbol{\rho}}^T \bar{\boldsymbol{A}}_k^H + \bar{\boldsymbol{A}}_k \hat{\boldsymbol{\rho}}^* \boldsymbol{a}_k^H + \bar{\boldsymbol{A}}_k \hat{\bar{\boldsymbol{R}}}_k \bar{\boldsymbol{A}}_k^H
$$
$$
+ \hat{\boldsymbol{R}}_e \tag{34}
$$

where $\hat{\boldsymbol{R}}_e = \boldsymbol{A} \hat{\boldsymbol{R}}_{sw} + \hat{\boldsymbol{R}}_{sw}^H \boldsymbol{A}^H + \hat{\boldsymbol{Q}}$, $\hat{\boldsymbol{\rho}} = (1/N) \sum_{n=1}^N s_k(n) \cdot \bar{\boldsymbol{s}}_k(n)$, $\hat{\bar{\boldsymbol{R}}}_k = (1/N) \sum_{n=1}^N \bar{\boldsymbol{s}}_k(n) \bar{\boldsymbol{s}}_k^H(n)$, while $\hat{\boldsymbol{R}}_{sw} = (1/N) \cdot \sum_{n=1}^N \boldsymbol{s}(n) \boldsymbol{w}^H(n)$, and the oblique projector $\boldsymbol{E}_{\bar{A}_k|\boldsymbol{a}_k}$ which projects onto the space $\mathcal{R}(\bar{\boldsymbol{A}}_k)$ along a direction parallel to the space $\mathcal{R}(\boldsymbol{a}_k)$ is given by (cf. [86], [91])

$$
\boldsymbol{E}_{\bar{A}_k|\boldsymbol{a}_k} \triangleq \bar{\boldsymbol{A}}_k (\bar{\boldsymbol{A}}_k^H \boldsymbol{\Pi}_{\boldsymbol{a}_k}^\perp \bar{\boldsymbol{A}}_k)^{-1} \bar{\boldsymbol{A}}_k^H \boldsymbol{\Pi}_{\boldsymbol{a}_k}^\perp \tag{35}
$$

where $\boldsymbol{\Pi}_{\boldsymbol{a}_k}^\perp \triangleq \boldsymbol{I}_{2M+1} - \boldsymbol{a}_k (\boldsymbol{a}_k^H \boldsymbol{a}_k)^{-1} \boldsymbol{a}_k^H$, $\boldsymbol{E}_{\bar{A}_k|\boldsymbol{a}_k} \bar{\boldsymbol{A}}_k = \bar{\boldsymbol{A}}_k$, and $\boldsymbol{E}_{\bar{A}_k|\boldsymbol{a}_k} \boldsymbol{a}_k = \boldsymbol{O}_{(2M+1)\times 1}$. Because the oblique projector with parameters in (35) is not available, by denoting the estimated electrical phase angles as $\{\hat{\psi}_k^{(t)}\}_{k=1}^K$ and $\{\hat{\phi}_k^{(t)}\}_{k=1}^K$, we can get an estimated oblique projector as $\hat{\boldsymbol{E}}_{\bar{A}_k|\boldsymbol{a}_k}^{(t)}$. Then, from (34) and (35), we get the projected correlation matrix $\hat{\boldsymbol{R}}_k^{(t)}$ as

$$
\hat{\boldsymbol{R}}_k^{(t)} = (\boldsymbol{I}_{2M+1} - \hat{\boldsymbol{E}}_{\bar{A}_k|\boldsymbol{a}_k}^{(t)}) \hat{\boldsymbol{R}} (\boldsymbol{I}_{2M+1} - \hat{\boldsymbol{E}}_{\bar{A}_k|\boldsymbol{a}_k}^{(t)})^H
$$
$$
\approx \hat{r}_{sk} \hat{\boldsymbol{a}}_k \hat{\boldsymbol{a}}_k^H. \tag{36}
$$

Obviously $\hat{\boldsymbol{R}}_k^{(t)}$ only contains the information of the signal $s_k(n)$. Thus, by estimating the electrical phase angles as discussed in Sections III.A and updating the index as $t = t + 1$, we can obtain the renewed estimates $\{\hat{\psi}_k^{(t+1)}\}_{k=1}^K$ and $\{\hat{\phi}_k^{(t+1)}\}_{k=1}^K$. This procedure should be repeated several times until the difference between two consecutive iterations becomes smaller than

a threshold, i.e.,

$$\sum_{k=1}^{K} \left| \hat{\psi}_k^{(t+1)} - \hat{\psi}_k^{(t)} \right| \le \varepsilon \qquad (37)$$

where ε is an arbitrary and positive small constant (e.g., $\varepsilon = 10^{-4}$), then finally we can obtain the refined estimates $\hat{\theta}_k$ and $\hat{r}_k$ of the source signal $s_k(n)$ from these $\hat{\psi}_k^{(t+1)}$ and $\hat{\phi}_k^{(t+1)}$.

Therefore when the finite array data are available, the proposed SLONS method can be implemented as follows:

1) Estimate the array covariance matrix as $\hat{\boldsymbol{R}} = (1/N)$ $\cdot \sum_{n=1}^{N} \boldsymbol{x}(n) \boldsymbol{x}^H(n)$.
   .... $10(2M+1)^2 N$ flops

2) Estimate $\{\gamma_{0k}\}_{k=1}^{K}$ by finding the phases of the K zeros of the polynomial $p_0(z)$ closest to the unit circle in the z-plane, where $p_0(z) \triangleq \boldsymbol{p}_0^H(z) \hat{\boldsymbol{U}}_{0n} \hat{\boldsymbol{U}}_{0n}^H \boldsymbol{p}_0(z)$, $\boldsymbol{p}_0(z) \triangleq [1, z^{-1}, \ldots, z^{-M}]^T$, and $z \triangleq e^{j2\gamma_0}$.
   .... $\mathcal{O}[(2M+1)^2 + (M+1)^3]$ flops

3) Estimate $\{\gamma_{2k}\}_{k=1}^{K}$ by finding the phases of the K zeros of the polynomial $p_2(z)$ closest to the unit circle in the z-plane, where $p_2(z) \triangleq \boldsymbol{p}_2^H(z) \hat{\boldsymbol{U}}_{2n} \hat{\boldsymbol{U}}_{2n}^H \boldsymbol{p}_2(z)$, $\boldsymbol{p}_2(z) \triangleq [1, z^{-1}, \ldots, z^{-(M-1)}]^T$, and $z \triangleq e^{j2\gamma_2}$.
   .... $\mathcal{O}[(2M-1)^2 + M^3]$ flops

4) Estimate and associate the electrical phase angles with (25) and (30), and denote them as $\{\hat{\psi}_k^{(t)}\}_{k=1}^{K}$ and $\{\hat{\phi}_k^{(t)}\}_{k=1}^{K}$, where $t = 0$.
   .... $16M^2 + 8M^2(M-K) + \mathcal{O}[M^3]$ flops

5) For $k = 1, 2, \ldots, K$, by calculating the oblique projector $\boldsymbol{E}_{\bar{\mathcal{A}}_k|\boldsymbol{a}_k}^{(t)}$ with (35) from $\{\hat{\psi}_k^{(t)}\}_{k=1}^{K}$ and $\{\hat{\phi}_k^{(t)}\}_{k=1}^{K}$, and the projected matrix $\hat{\boldsymbol{R}}_k^{(t)}$ with (36), estimate the renewed electrical phase angles $\{\hat{\psi}_k^{(t+1)}\}_{k=1}^{K}$ and $\{\hat{\phi}_k^{(t+1)}\}_{k=1}^{K}$ with (19) and (29)-(30).
   .... $16(2M+1)^3 + (2M+1)^2(24K - 23) + 8(2M+1)(2(K-1)^2 + 1) + \mathcal{O}[(2M+1)^2 + (M+1)^3]$ flops

6) If the condition in (37) is not satisfied, repeat Step 5 by setting $t = t+1$; otherwise by reexpressing the estimates $\{\hat{\psi}_k^{(t+1)}\}_{k=1}^{K}$ and $\{\hat{\phi}_k^{(t+1)}\}_{k=1}^{K}$ as $\{\hat{\psi}_k\}_{k=1}^{K}$ and $\{\hat{\phi}_k\}_{k=1}^{K}$, estimate the DOAs $\{\hat{\theta}_k\}_{k=1}^{K}$ and ranges $\{\hat{r}_k\}_{k=1}^{K}$ with (31) and (32).

The computational complexity of each step is roughly indicated in terms of the number of MATLAB flops, where a flop is defined as a floating-point additional or multiplication operation,[1] and hence the computational complexity of the SLONS is approximately $10(2M+1)^2 N + 16(2M+1)^3 N_i$ if $2M + 1 \gg K$ flops, which occurs often in applications of array processing, where N_i denotes the times of iteration ($N_i \ge 1$).

Remark B: The quantitative comparisons of computational complexities between the SLONS and some existing localization methods for the near-field sources in the additive uniform noise

---

[1] Such as the computational complexities of $\boldsymbol{X} \pm \boldsymbol{Y}$ and $\boldsymbol{XY}$ ($\boldsymbol{X}$ and $\boldsymbol{Y}$ are $L \times M$ and $M \times N$ complex matrices, respectively) are $2LM$ and $8LMN$, respectively. See more details about the calculation of the computational complexity in [47] and references therein.
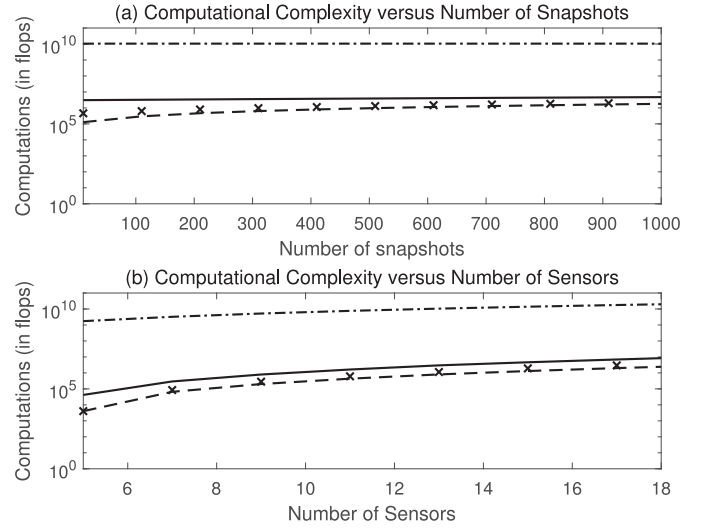

Fig. 2. Comparison of computational complexities in MATLAB flops versus (a) the number of snapshots ($2M + 1 = 11$) and (b) the number of sensors ($N = 200$) (dot-dashed line: 2D-MUSIC; "x": WLPM; solid line: the SLONS with 10 iterations; and dashed line: the SLONS w/o iteration).

such as the modified 2D-MUSIC [15] and the weighted linear prediction method (WLPM) [23] are shown in Fig. 2. The 2D-MUSIC is based on the spherical wavefront model and involves 2D spectrum peak searching, hence its computational complexity is about $10(2M+1)^2 N + (8(2M+1)^2 + 8(2M+1))(180/\Delta\theta)((2D^2/\lambda - 0.62(D^3/\lambda)^{1/2})/\Delta r) + \mathcal{O}[(2M+1)^3]$ flops, where $\Delta\theta$ and Δr are the angular and range grid spacings (i.e., $\Delta\theta = 0.002°$ and $\Delta r = 0.002\lambda$), and the precise peak searching necessitates fine grid spacing, but it is a rather time-consuming task with heavy computational load. On the contrary, the WLPM is based on the Fresnel approximation of the spherical wavefront model, and its computational complexity is reduced roughly to $10(2M+1)^2 N + \mathcal{O}[(2M+1-K)^3]$ flops. From Fig. 2, we can see that the proposed SLONS is computationally more efficient than the 2D-MUSIC and similar to the WLPM. □

Remark C: The $2M+1$, $2M$ and $2M-1$ correlations along three different anti-diagonals of $\hat{\boldsymbol{R}}$ are used to construct three Toeplitz matrices with the dimensions $(M+1) \times (M+1)$, $M \times M$, and $M \times M$, and hence the maximum resolvable signals of the SLONS is $K < M$. This is roughly the same as the WLPM [23] and other subspace-based near-field localization methods (e.g., [24], [92], [93]), where the geometric symmetry of the uniform linear sensor array is exploited to facilitate the parameter estimation (cf. [94]). □

IV. STOCHASTIC CRB FOR NEAR-FIELD SOURCES IN UNKNOWN SPATIALLY NONUNIFORM NOISE

The CRB provides a lower bound on the variance of any unbiased estimator (see, e.g., [95]). Although the expressions of the stochastic and deterministic CRBs were studied for the far-field sources under the nonuniform noise assumption [57], [100], [101], and some expressions of the stochastic and deterministic CRBs were derived for the near-field sources

in the spatially uniform noise environment [16], [23], [96]–[99], to the best of our knowledge, the CRB for the near-field source localization in the spatially nonuniform noises is still unavailable so far. Therefore, we derive the closed-form stochastic CRB for the estimated DOAs and ranges of the near-field sources in the presence of spatially nonuniform noises herein.

Under the data model assumptions, the Fisher information matrix (FIM) for a parameter vector $\boldsymbol{\alpha}$ is given by (e.g., [95], [100]–[102])

$$(\text{FIM})_{k,l} = N \text{tr} \left\{ \frac{\partial \boldsymbol{R}}{\partial \boldsymbol{\alpha}_k} \boldsymbol{R}^{-1} \frac{\partial \boldsymbol{R}}{\partial \boldsymbol{\alpha}_l} \boldsymbol{R}^{-1} \right\} \tag{38}$$

for $k, l = 1, 2, \ldots, 3K + 2M + 1$, where $\boldsymbol{\alpha} \triangleq [\boldsymbol{\zeta}^T, \boldsymbol{\rho}^T, \boldsymbol{\sigma}^T]^T$, $\boldsymbol{\zeta} \triangleq [\theta_1, \theta_2, \ldots, \theta_K, r_1, r_2, \ldots, r_K]^T$, $\boldsymbol{\rho} \triangleq [r_{s_1}, r_{s_2}, \ldots, r_{s_K}]^T$, and $\boldsymbol{\sigma} \triangleq [\sigma_1^2, \sigma_2^2, \ldots, \sigma_{2M+1}^2]^T$. To focus only on the desired $\boldsymbol{\zeta}$-block of the CRB $= \text{FIM}^{-1}$, which is denoted by $\text{CRB}(\boldsymbol{\zeta})$, we can obtain a closed-form expression of the CRB for the estimated DOAs and ranges of the near-field sources as the following theorem.

Theorem 1: The $2K \times 2K$ stochastic CRB for the location parameters of the near-field sources under unknown spatially nonuniform noise environment is given by

$$\text{CRB}(\boldsymbol{\zeta}) = \frac{1}{N} \left(\boldsymbol{F} - \boldsymbol{H} \boldsymbol{K}^{-1} \boldsymbol{H}^T \right)^{-1} \tag{39}$$

where

$$\boldsymbol{F} = 2\text{Re} \left\{ (\tilde{\boldsymbol{D}}^H \boldsymbol{\Pi}_{\tilde{A}}^{\perp} \tilde{\boldsymbol{D}}) \odot (\boldsymbol{J} \otimes (\boldsymbol{R}_s \tilde{\boldsymbol{A}}^H \tilde{\boldsymbol{R}}^{-1} \tilde{\boldsymbol{A}} \boldsymbol{R}_s)^T) \right\} \tag{40}$$

$$\boldsymbol{H} = 2\text{Re} \left\{ (\tilde{\boldsymbol{D}}^H \boldsymbol{\Pi}_{\tilde{A}}^{\perp}) \odot (\boldsymbol{1} \otimes (\tilde{\boldsymbol{R}}^{-1} \tilde{\boldsymbol{A}} \boldsymbol{R}_s)^T) \right\} \tag{41}$$

$$\boldsymbol{K} = 2\text{Re} \left\{ \boldsymbol{\Pi}_{\tilde{A}}^{\perp} \odot \tilde{\boldsymbol{R}}^{-T} \right\} - \boldsymbol{\Pi}_{\tilde{A}}^{\perp} \odot (\boldsymbol{\Pi}_{\tilde{A}}^{\perp})^T \tag{42}$$

while $\tilde{\boldsymbol{R}} \triangleq \boldsymbol{Q}^{-1/2} \boldsymbol{R} \boldsymbol{Q}^{-1/2}$, $\tilde{\boldsymbol{A}} \triangleq \boldsymbol{Q}^{-1/2} \boldsymbol{A}$, $\tilde{\boldsymbol{D}} = \boldsymbol{Q}^{-1/2} \boldsymbol{D}$, $\boldsymbol{\Pi}_{\tilde{A}}^{\perp} \triangleq \boldsymbol{I}_{2M+1} - \tilde{\boldsymbol{A}} (\tilde{\boldsymbol{A}}^H \tilde{\boldsymbol{A}})^{-1} \tilde{\boldsymbol{A}}^H$, $\boldsymbol{1} \triangleq [1, 1]^T$, $\boldsymbol{J} \triangleq \boldsymbol{1} \boldsymbol{1}^T$, and $\boldsymbol{D} \triangleq [\boldsymbol{d}_{\theta_1}, \boldsymbol{d}_{\theta_2}, \ldots, \boldsymbol{d}_{\theta_K}, \boldsymbol{d}_{r_1}, \boldsymbol{d}_{r_2}, \ldots, \boldsymbol{d}_{r_K}]$, in which $\boldsymbol{d}_{\theta_k} \triangleq \partial \boldsymbol{a}(\theta_k, r_k) / \partial \theta_k$ and $\boldsymbol{d}_{r_k} \triangleq \partial \boldsymbol{a}(\theta_k, r_k) / \partial r_k$.

Proof: See Appendix. ∎

V. NUMERICAL EXAMPLES

Here we evaluate the effectiveness of the proposed SLONS through numerical examples. The uniform linear sensor array consists of $2M + 1 = 11$ sensors with element spacing $d = \lambda/4$, while the complex incident signals $\{s_k(n)\}$ are generated by

$$s_k(n) = s_k^r(n) + j s_k^i(n) \tag{43}$$

where the real part $s_k^r(n)$ and the imaginary part $s_k^i(n)$ are two different random processes given by Matlab Random Number Generator function "randn". The SNR is defined as

$$\text{SNR} = 10 \log_{10} \frac{1}{2M+1} \sum_{m=-M}^{M} \frac{\sigma_m^2}{r_s} \tag{44}$$

where the incident signals have the same power, i.e., $r_{s_1} = \cdots = r_{s_K} = r_s$. The 2D-MUSIC [15] and the WLPM [23] are carried
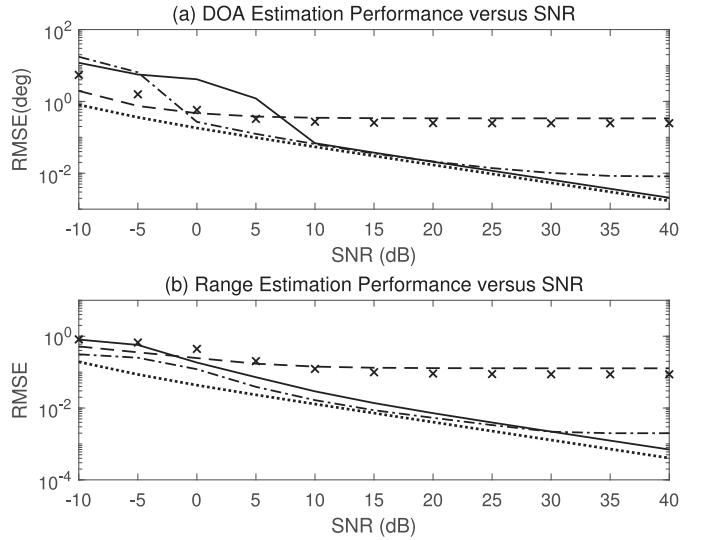

Fig. 3. RMSE of the estimated DOAs and ranges versus the SNR ("x": WLPM; dot-dashed line: 2D-MUSIC; dashed line: the SLONS w/o iteration; solid line: the SLONS; dotted line: CRB) in Example 1.

out, and the stochastic CRB derived in (39) is calculated for performance comparison. The angular and range grid spacings $\Delta\theta$ and Δr are fixed at $\Delta\theta = 0.09°$ and $\Delta r = 0.09\lambda$ for the 2D-MUSIC, the iteration threshold in (37) is set at $\varepsilon = 10^{-6}$. The results are all based on 1000 independent trials (i.e., $\bar{N} = 1,000$).

Example 1–Performance versus SNR: There are three near-field sources with equal power located at $(-11°, 2.9\lambda)$, $(21°, 3.0\lambda)$, and $(47°, 3.3\lambda)$. The number of snapshots is $N = 500$, and the SNR is varied from -10dB to 40 dB, where the covariance matrix of additive noises is given by

$$\boldsymbol{Q} = \sigma_n \text{diag}(2, 2, 0.7, 1, 1.5, 5, 3, 3.6, 4, 2, 3). \tag{45}$$

The averaged empirical root mean-squared-errors (RMSEs) of the estimated location parameters in terms of the SNR are plotted in Figs. 3(a) and 3(b). The 2D-MUSIC [15] utilizes all $(2M+1)^2$ correlations of $\hat{\boldsymbol{R}}$, and it is rather time-consuming but its performance is restricted by the angular/range grid spacing, while the WLPM [23] uses the $2M+1$, $2M$ and $2M$ correlations along three anti-diagonals of $\hat{\boldsymbol{R}}$ with a rather low computational cost, but it is rather complicated to determine the optimal weighting matrix. Moreover, the structure properties of the array covariance matrices of the incident signals and the additive noise are required in the 2D-MUSIC and the WLPM, but the structure properties are only valid for large number of snapshots. When the number of snapshots is not sufficiently large enough, the erroneous estimated correlations will cause the linear prediction (LP) model to be invalid, and correspondingly the WLPM suffers severely "saturation behavior" regardless of the SNR as shown in Fig. 3, where the estimated DOAs and ranges have high elevate error floors and will not decrease with the increasing SNR. The 2D-MUSIC has relatively good performance at low and moderate SNRs, but the estimation errors of the DOAs and ranges no longer decrease at high SNR

due to the limited searching grids of the 2D spectrum. Although the saturation behavior of the 2D-MUSIC could be alleviated by a refined searching grid, the amount of computational load will increase dramatically. In this paper, since the range space of each incident signal is nonoverlapping and not orthogonal to that of the others, the oblique projection operator (see, e.g., [86]) is used to isolate one signal from the others, and an alternating iterative scheme is presented to improve the performance with finite snapshots of array data, where the location parameters (i.e., two electric angles) of one source are estimated in one iteration, and the mutual influence between the multiple near-field sources are eliminated. As shown in Figs. 3(a) and 3(b), we can find that the SLONS has a good tradeoff between the computational complexity and the estimation performance compared with the 2D-MUSIC [15] and is superior to the WLPM [23], where its empirical RMSEs of the estimated DOAs and ranges are very close to the CRBs at moderate and high SNRs, and the "saturation behavior" is overcome effectively. Unfortunately, the SLONS performs poorly at relatively low SNR because only some (but not all) correlations are used compared with the 2D-MUSIC.

Example 2–Performance versus Number of Snapshots: The simulation conditions are similar to those in Example 1, except that the SNR is fixed at 20 dB and the number of snapshots varies from 100 to 10,000.

Figs. 4(a) and 4(b) show the averaged empirical RMSEs of the estimated DOAs and ranges with respect to the number of snapshots. Since the WLPM uses the similar correlations along three anti-diagonals of the array covariance matrix, its performance is similar to the SLONS without iteration, and although the RMSEs of the estimated DOAs and ranges decrease with the increasing number of snapshots, these RMSEs cannot reach the corresponding CRBs due to "saturation behavior". Additionally as described in Example 1, owing to the limited searching grips of the 2D spectrum, the RMSEs of the 2D-MUSIC deviate from the CRBs even for larger number of snapshots. As shown in Figs. 4(a) and 4(b), when the number of snapshots is not large, the estimates initial values of the electric angles used for the iteration may have a large deviation, and the iteration may not converge, hence the SLONS will have relatively lager estimation error. However when the number of snapshots is larger, the SLONS with iteration outperforms the WLPM for both the estimation of DOAs and ranges, where the "saturation behavior" is alleviated.

Example 3–Convergence Behavior: The simulation conditions are similar to those in above examples, and the averaged convergence behaviors of the proposed alternating iterative scheme are plotted in Fig. 5 for different SNR and number of snapshots.

From Fig. 5, we can see that the alternating iterative scheme converges within roughly 20 times of iterations and the "saturation behavior" can be resolved for small number of snapshots, while the convergence can be obtained in a few iterations and the performance is improved remarkably for sufficiently large number of snapshots. However, the convergence analysis of the alternating iterative scheme is rather complicated, and the
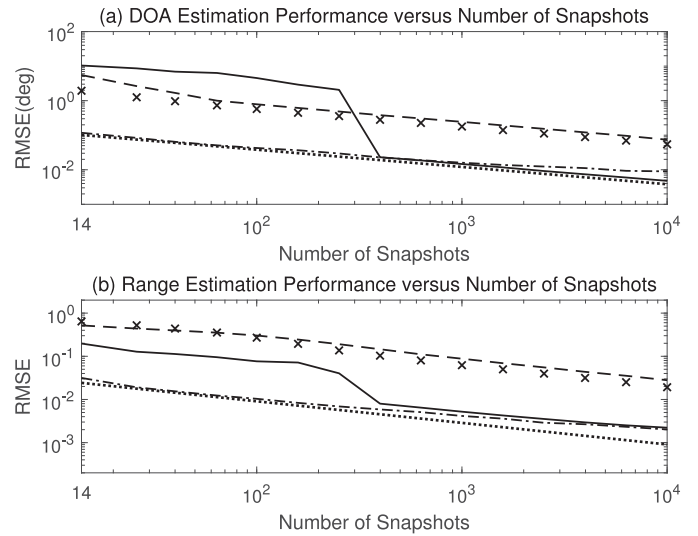

Fig. 4. RMSE of the estimated DOAs and ranges versus the number of snapshots ("x": WLPM; dot-dashed line: 2D-MUSIC; dashed line: the SLONS w/o iteration; solid line: the SLONS; dotted line: CRB) in Example 2.
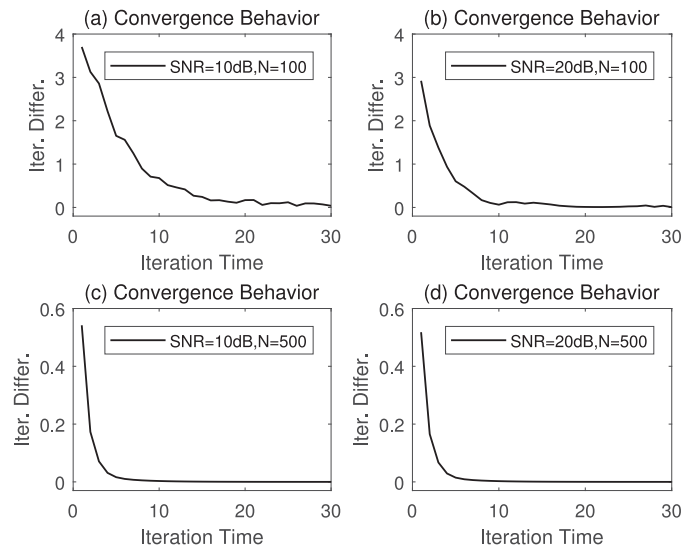
Fig. 5. Averaged convergence behaviors of the alternating iterative scheme for several SNRs and numbers of snapshots in Example 3.

convergence depends on the initialization of $\{\hat{\psi}_k^{(0)}\}_{k=1}^K$ and $\{\hat{\phi}_k^{(0)}\}_{k=1}^K$.

Example 4—Performance versus Angular Separation: In this example, two near-field sources are located at $(11^\circ, 2.9\lambda)$ and $(11^\circ + \Delta\theta, 2.9\lambda)$, where $\Delta\theta$ is varied from 0.5° to 19.5° with $\Delta\theta = 1^\circ$, and the SNR is fixed at 15 dB, and the number of snapshots is set at $N = 500$.

Fig. 6 displays the averaged empirical RMSEs of the estimated DOAs and ranges against the angular separation. We can find that the proposed SLONS generally outperforms the WLPM and the 2D-MUSIC for the closely-spaced sources, and the RMSEs of the location parameters do not decrease monotonically with

Fig. 6. RMSEs of (a) the estimated DOAs versus the angular separation and (b) the estimated ranges versus the angular separation for Example 4 ("x": WLPM; dot-dashed line: 2D-MUSIC; dashed line: the SLONS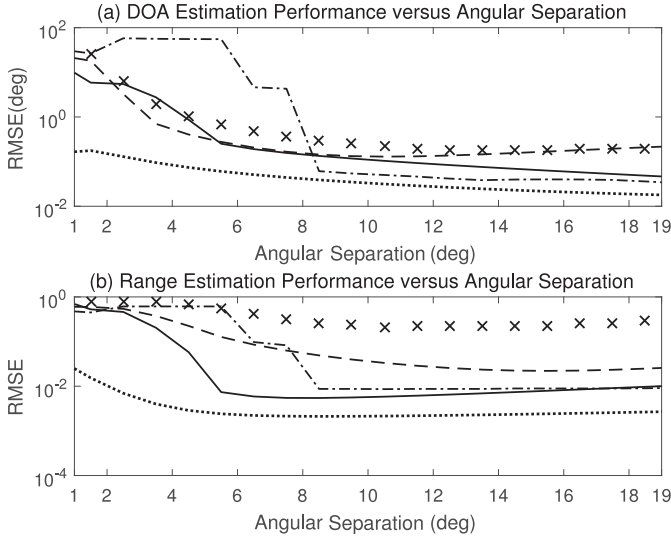 w/o iteration; solid line: the SLONS; dotted line: CRB) (SNR $= 15$dB, $N = 500$, $(11°, 2.9\lambda)$, and $(11° + \Delta\theta, 2.9\lambda)$).
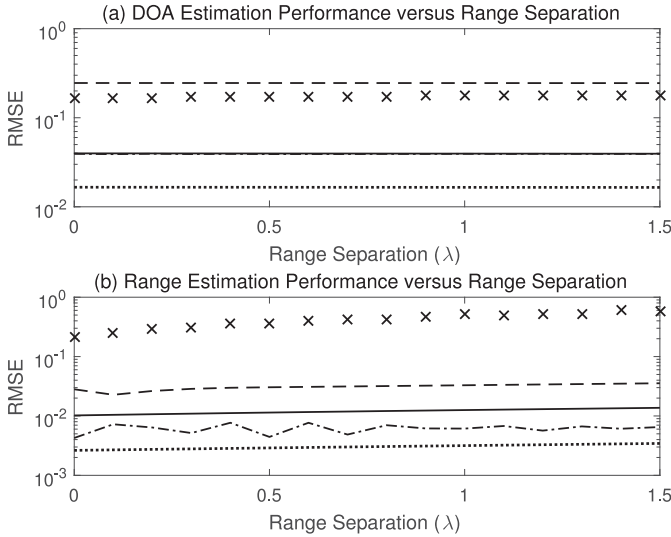

Fig. 7. RMSEs of (a) the estimated DOAs versus the range separation and (b) the estimated ranges versus the range separation for Example 4 ("x": WLPM; dot-dashed line: 2D-MUSIC; dashed line: the SLONS w/o iteration; solid line: the SLONS; dotted line: CRB) (SNR $= 15$dB, $N = 500$, $(11°, 2.9\lambda)$, and $(11° + \Delta\theta, 2.9\lambda + \Delta\lambda)$).

the increasing angular separation. It is also worth mentioning that the proposed SLONS is computationally more efficient than the 2D-MUSIC, though its performance of the DOA estimation is worse than the 2D-MUSIC for some large angular separations.

Example 5—Performance versus Range Separation: The simulation conditions are similar to those in Example 4, while two near-field sources are located at $(11°, 2.9\lambda)$ and $(11°, 2.9\lambda + \Delta\lambda)$, where $\Delta\lambda$ is varied from 0λ to 1.5λ with $\Delta\bar{\lambda} = 0.1\lambda$.

Fig. 7 demonstrates the averaged empirical RMSEs of the estimated location parameters in terms of the range separation. When the source range increases, the electric angle ϕ_k in (5) will become very small, and the estimation performance of ϕ_k will be an ill-posed problem [23]. Hence the range estimation performance will become wore from (32), while the DOA estimation performance is almost constant, where the estimation performance is mainly dominated by the number of snapshots and SNR. Obviously the estimation performance of the proposed SLONS is effectively improved by using the iteration, and the SLONS is superior to the WLPM for both DOA and range estimation. Additionally the SLONS has similar DOA estimation performance but poor range estimation performance compared with the 2D-MUSIC in this empirical scenario.

It should be noted that the empirical RMSEs of the DOA and range estimates do not decrease monotonically as the range separation increases. Furthermore the SLONS can be extended to the multiple far-field sources in presence of unknown nonuniform noises, where the source location is characterized only by the DOA.

VI. CONCLUSION

A new subspace-based method called SLONS was proposed for localization of multiple near-field sources impinging on a symmetric uniform linear sensor array in the unknown spatially additive nonuniform noises. A new pari-matching scheme was developed, and an oblique projector based alternating iterative scheme was presented to combat the "saturation behavior" due to finite number of snapshots. Further the closed-form stochastic CRB was derived for the localization of near-field sources in unknown nonuniform noises explicitly. The simulation results showed that the proposed method has remarkable estimation performance.

APPENDIX PROOF OF THEOREM 1

The derivation of the CRB will use the following readily-checked facts (see, e.g., [104])

$$\text{tr}\{\boldsymbol{XY}\} = \text{vec}^H(\boldsymbol{X}^H)\text{vec}(\boldsymbol{Y}) \tag{A1}$$

$$\text{vec}\{\boldsymbol{XYZ}\} = (\boldsymbol{Z}^T \otimes \boldsymbol{X})\text{vec}(\boldsymbol{Y}) \tag{A2}$$

which hold for any conformable matrices $\boldsymbol{X}, \boldsymbol{Y}$, and $\boldsymbol{Z}$. By using (A1) and (A2), the matrix FIM associated with the data model in (6) can be expressed as (cf. [101], [102])

$$\text{FIM} = N \left(\frac{d\boldsymbol{y}}{d\boldsymbol{\alpha}^T}\right)^H (\boldsymbol{R}^{-T} \otimes \boldsymbol{R}^{-1}) \left(\frac{d\boldsymbol{y}}{d\boldsymbol{\alpha}^T}\right) \tag{A3}$$

where $\boldsymbol{y} = \text{vec}\{\boldsymbol{R}\} = (\boldsymbol{A}^* \otimes \boldsymbol{A})\text{vec}(\boldsymbol{R}_s) + \text{vec}(\boldsymbol{Q})$. By defining the following two matrices as

$$\boldsymbol{G} \triangleq (\boldsymbol{R}^{-T/2} \otimes \boldsymbol{R}^{-1/2}) \frac{d\boldsymbol{y}}{d\boldsymbol{\zeta}^T} \tag{A4}$$

$$\boldsymbol{\Delta} \triangleq (\boldsymbol{R}^{-T/2} \otimes \boldsymbol{R}^{-1/2}) \left[\frac{d\boldsymbol{y}}{d\boldsymbol{\rho}^T}, \frac{d\boldsymbol{y}}{d\boldsymbol{\sigma}^T}\right] \tag{A5}$$

from (A3), we can obtain

$$\frac{1}{N}\text{FIM} = \begin{bmatrix} \boldsymbol{G}^H \\ \boldsymbol{\Delta}^H \end{bmatrix} [\boldsymbol{G}, \boldsymbol{\Delta}] \qquad (A6)$$

and hence the CRB for the parameter $\boldsymbol{\zeta}$ consisting of the DOAs and ranges of near-field sources under unknown nonuniform noise environment is given by (cf. [101], [102])

$$\text{CRB}(\boldsymbol{\zeta}) = \frac{1}{N}\text{FIM}^{-1} = \frac{1}{N}(\boldsymbol{G}^H\boldsymbol{\Pi}_\Delta^\perp\boldsymbol{G})^{-1} \qquad (A7)$$

where $\boldsymbol{\Pi}_\Delta^\perp = \boldsymbol{I} - \boldsymbol{\Pi}_\Delta$, and $\boldsymbol{\Pi}_\Delta \triangleq \boldsymbol{\Delta}(\boldsymbol{\Delta}^H\boldsymbol{\Delta})^{-1}\boldsymbol{\Delta}^H$, while $\boldsymbol{\Pi}_\Delta$ and $\boldsymbol{\Pi}_\Delta^\perp$ stand for the orthogonal projection matrices onto the range space of $\boldsymbol{\Delta}$ and its orthogonal complement, respectively, and the inversion of partitioned matrices [103] is used implicitly. Further by partitioning the matrix $\boldsymbol{\Delta}$ in (A5) into two submatrices as

$$\boldsymbol{\Delta} = [\boldsymbol{V}, \boldsymbol{U}] \qquad (A8)$$

where

$$\boldsymbol{V} \triangleq (\boldsymbol{R}^{-T/2} \otimes \boldsymbol{R}^{-1/2})\frac{d\boldsymbol{y}}{d\boldsymbol{\rho}^T} \qquad (A9)$$

$$\boldsymbol{U} \triangleq (\boldsymbol{R}^{-T/2} \otimes \boldsymbol{R}^{-1/2})\frac{d\boldsymbol{y}}{d\boldsymbol{\sigma}^T}. \qquad (A10)$$

Since the matrices $\boldsymbol{\Delta}$ and $[\boldsymbol{V}, \boldsymbol{\Pi}_V^\perp\boldsymbol{U}]$ have the same range space, $\boldsymbol{\Pi}_\Delta^\perp$ in (A7) is easily given by (cf. [101], [102])

$$\boldsymbol{\Pi}_\Delta^\perp = \boldsymbol{\Pi}_V^\perp - \boldsymbol{\Pi}_V^\perp\boldsymbol{U}(\boldsymbol{U}^H\boldsymbol{\Pi}_V^\perp\boldsymbol{U})^{-1}\boldsymbol{U}^H\boldsymbol{\Pi}_V^\perp. \qquad (A11)$$

Now by reexpressing the parameter $\boldsymbol{\zeta}$ in (38) as $\boldsymbol{\zeta} = [\boldsymbol{\theta}^T, \boldsymbol{r}^T]^T$, where $\boldsymbol{\theta} \triangleq [\theta_1, \theta_2, \ldots, \theta_K]^T$, and $\boldsymbol{r} \triangleq [r_1, r_2, \ldots, r_K]^T$, the matrix $\boldsymbol{G}$ in (A4) can be rewritten as

$$\boldsymbol{G} = (\boldsymbol{R}^{-T/2} \otimes \boldsymbol{R}^{-1/2}) \left[\frac{d\boldsymbol{y}}{d\boldsymbol{\theta}^T}, \frac{d\boldsymbol{y}}{d\boldsymbol{r}^T}\right] = [\boldsymbol{G}_\theta, \boldsymbol{G}_r] \qquad (A12)$$

where

$$\boldsymbol{G}_\theta \triangleq (\boldsymbol{R}^{-T/2} \otimes \boldsymbol{R}^{-1/2})\frac{d\boldsymbol{y}}{d\boldsymbol{\theta}^T} \qquad (A13)$$

$$\boldsymbol{G}_r \triangleq (\boldsymbol{R}^{-T/2} \otimes \boldsymbol{R}^{-1/2})\frac{d\boldsymbol{y}}{d\boldsymbol{r}^T}. \qquad (A14)$$

Then by substituting (A8)-(A14) into (A7), after some manipulations, we can obtain

$$\text{CRB}(\boldsymbol{\zeta})$$
$$= \frac{1}{N}\left(\boldsymbol{F} - \boldsymbol{H}\boldsymbol{K}^{-1}\boldsymbol{H}^T\right)^{-1}$$
$$= \frac{1}{N}\begin{bmatrix} \boldsymbol{F}_{\theta\theta} - \boldsymbol{H}_\theta\boldsymbol{K}^{-1}\boldsymbol{H}_\theta^H, & \boldsymbol{F}_{\theta r} - \boldsymbol{H}_\theta\boldsymbol{K}^{-1}\boldsymbol{H}_r^H \\ \boldsymbol{F}_{\theta r}^H - \boldsymbol{H}_r\boldsymbol{K}^{-1}\boldsymbol{H}_\theta^H, & \boldsymbol{F}_{rr} - \boldsymbol{H}_r\boldsymbol{K}^{-1}\boldsymbol{H}_r^H \end{bmatrix}^{-1}$$

$$(A15)$$

where

$$\boldsymbol{F} \triangleq \boldsymbol{G}^H\boldsymbol{\Pi}_V^\perp\boldsymbol{G} \qquad (A16)$$

$$\boldsymbol{H} \triangleq \boldsymbol{G}^H\boldsymbol{\Pi}_V^\perp\boldsymbol{U} \qquad (A17)$$

$$\boldsymbol{K} \triangleq \boldsymbol{U}^H\boldsymbol{\Pi}_V^\perp\boldsymbol{U} \qquad (A18)$$

while

$$\boldsymbol{F}_{\theta\theta} \triangleq \boldsymbol{G}_\theta^H\boldsymbol{\Pi}_V^\perp\boldsymbol{G}_\theta \qquad (A19)$$

$$\boldsymbol{F}_{\theta r} \triangleq \boldsymbol{G}_\theta^H\boldsymbol{\Pi}_V^\perp\boldsymbol{G}_r \qquad (A20)$$

$$\boldsymbol{F}_{rr} \triangleq \boldsymbol{G}_r^H\boldsymbol{\Pi}_V^\perp\boldsymbol{G}_r \qquad (A21)$$

$$\boldsymbol{H}_\theta \triangleq \boldsymbol{G}_\theta^H\boldsymbol{\Pi}_V^\perp\boldsymbol{U} \qquad (A22)$$

$$\boldsymbol{H}_r \triangleq \boldsymbol{G}_r^H\boldsymbol{\Pi}_V^\perp\boldsymbol{U} \qquad (A23)$$

where the property $\boldsymbol{F}_{r\theta} = \boldsymbol{F}_{\theta r}^H$ is used in (A15).

Further we need to calculate the derivatives of $\boldsymbol{y}$ with respect to $\{\theta_k, r_k\}$. First, we consider $d\boldsymbol{y}/d\boldsymbol{\theta}^T$ and $d\boldsymbol{y}/d\boldsymbol{r}^T$. Let $\boldsymbol{p}_k$ denote the kth column of signal covariance matrix $\boldsymbol{R}_s$, i.e. $\boldsymbol{R}_s = [\boldsymbol{p}_1, \boldsymbol{p}_2, \ldots, \boldsymbol{p}_K]$. Thus, we have

$$\frac{d\boldsymbol{R}}{d\theta_k} = \boldsymbol{d}_{\theta_k}\boldsymbol{p}_k^H\boldsymbol{A}^H + \boldsymbol{A}\boldsymbol{p}_k\boldsymbol{d}_{\theta_k} \qquad (A24)$$

$$\frac{d\boldsymbol{R}}{dr_k} = \boldsymbol{d}_{r_k}\boldsymbol{p}_k^H\boldsymbol{A}^H + \boldsymbol{A}\boldsymbol{p}_k\boldsymbol{d}_{r_k} \qquad (A25)$$

Therefore, the kth column of $\boldsymbol{G}$ (i.e, $\boldsymbol{G}_\theta$ and $\boldsymbol{G}_r$) is given by

$$\boldsymbol{g}_{\theta_k} = \text{vec}\left(\boldsymbol{R}^{-1/2}\frac{d\boldsymbol{R}}{d\theta_k}\boldsymbol{R}^{-1/2}\right) \triangleq \text{vec}(\boldsymbol{Z}_{\theta_k} + \boldsymbol{Z}_{\theta_k}^H) \quad (A26)$$

$$\boldsymbol{g}_{r_k} = \text{vec}\left(\boldsymbol{R}^{-1/2}\frac{d\boldsymbol{R}}{dr_k}\boldsymbol{R}^{-1/2}\right) \triangleq \text{vec}(\boldsymbol{Z}_{r_k} + \boldsymbol{Z}_{r_k}^H) \quad (A27)$$

where

$$\boldsymbol{Z}_{\theta_k} = \boldsymbol{R}^{-1/2}\boldsymbol{A}\boldsymbol{p}_k\boldsymbol{d}_{\theta_k}^H\boldsymbol{R}^{-1/2} \qquad (A28)$$

$$\boldsymbol{Z}_{r_k} = \boldsymbol{R}^{-1/2}\boldsymbol{A}\boldsymbol{p}_k\boldsymbol{d}_{r_k}^H\boldsymbol{R}^{-1/2} \qquad (A29)$$

Then we consider $d\boldsymbol{y}/d\boldsymbol{\rho}^T$. The derivation of this part is similar to the far-field case (e.g., [57]). Thus by using the following properties

$$\boldsymbol{\Pi}_V^\perp = \boldsymbol{\Pi}_{(\boldsymbol{R}^{-1/2}A)^*\otimes(\boldsymbol{R}^{-1/2}A)}^\perp \qquad (A30)$$

$$\boldsymbol{\Pi}_{(X\otimes Y)} = \boldsymbol{I} \otimes \boldsymbol{\Pi}_Y^\perp + \boldsymbol{\Pi}_X^\perp \otimes \boldsymbol{I} - \boldsymbol{\Pi}_X^\perp \otimes \boldsymbol{\Pi}_Y^\perp \qquad (A31)$$

From (A26)–(A31), we obtain

$$\boldsymbol{\Pi}_V^\perp\boldsymbol{g}_{\theta_k} = \text{vec}\left(\boldsymbol{\Pi}_{\boldsymbol{R}^{-1/2}A}^\perp\boldsymbol{Z}_{\theta_k}^H + \boldsymbol{Z}_{\theta_k}\boldsymbol{\Pi}_{\boldsymbol{R}^{-1/2}A}^\perp\right) \qquad (A32)$$

$$\boldsymbol{\Pi}_V^\perp\boldsymbol{g}_{r_k} = \text{vec}\left(\boldsymbol{\Pi}_{\boldsymbol{R}^{-1/2}A}^\perp\boldsymbol{Z}_{r_k}^H + \boldsymbol{Z}_{r_k}\boldsymbol{\Pi}_{\boldsymbol{R}^{-1/2}A}^\perp\right) \qquad (A33)$$

where the following facts are used

$$\boldsymbol{\Pi}_{\boldsymbol{R}^{-1/2}A}^\perp\boldsymbol{Z}_{\theta_k} = \boldsymbol{O}_{(2M+1)\times(2M+1)} \qquad (A34)$$

$$\boldsymbol{\Pi}_{\boldsymbol{R}^{-1/2}A}^\perp\boldsymbol{Z}_{r_k} = \boldsymbol{O}_{(2M+1)\times(2M+1)} \qquad (A35)$$

Finally, from (A19)–(A21) along with (A1), (A26), (A27), (A32), and (A33), the (i,k)th element of $\boldsymbol{F}$ can be obtained as

$$(\boldsymbol{F}_{\theta\theta})_{i,k} = 2\text{Re}\left\{\text{tr}\left(\boldsymbol{Z}_{\theta_i}\boldsymbol{\Pi}_{\boldsymbol{R}^{-1/2}A}^\perp\boldsymbol{Z}_{\theta_k}^H\right)\right\} \qquad (A36)$$

$$(\boldsymbol{F}_{\theta r})_{i,k} = 2\text{Re}\left\{\text{tr}\left(\boldsymbol{Z}_{\theta_i}\boldsymbol{\Pi}_{\boldsymbol{R}^{-1/2}A}^\perp\boldsymbol{Z}_{r_k}^H\right)\right\} \qquad (A37)$$

$$(\boldsymbol{F}_{rr})_{i,k} = 2\text{Re}\left\{\text{tr}\left(\boldsymbol{Z}_{r_i}\boldsymbol{\Pi}_{\boldsymbol{R}^{-1/2}A}^\perp\boldsymbol{Z}_{r_k}^H\right)\right\} \qquad (A38)$$

Furthermore, we can easily have

$$\boldsymbol{R}^{-1/2}\boldsymbol{\Pi}_{\boldsymbol{R}^{-1/2}A}^\perp\boldsymbol{R}^{-1/2} = \boldsymbol{Q}^{-1/2}\tilde{\boldsymbol{\Pi}}_{\tilde{\boldsymbol{A}}}^\perp\boldsymbol{Q}^{-1/2} \triangleq \tilde{\boldsymbol{\Pi}}_{\tilde{\boldsymbol{A}}}^\perp \qquad (A39)$$

By inserting (A28) and (A29) into (A36)–(A38) and then using (A39) yields

$$(\boldsymbol{F}_{\theta\theta})_{i,k} = 2\mathrm{Re}\{(\boldsymbol{d}_{\theta_i}\tilde{\boldsymbol{\Pi}}_{\boldsymbol{A}}^{\perp}\boldsymbol{d}_{\theta_k})(\boldsymbol{p}_k^H \boldsymbol{A}^H \boldsymbol{R}^{-1}\boldsymbol{A}\boldsymbol{p}_i)\} \quad (A40)$$

$$(\boldsymbol{F}_{\theta r})_{i,k} = 2\mathrm{Re}\{(\boldsymbol{d}_{\theta_i}\tilde{\boldsymbol{\Pi}}_{\boldsymbol{A}}^{\perp}\boldsymbol{d}_{r_k})(\boldsymbol{p}_k^H \boldsymbol{A}^H \boldsymbol{R}^{-1}\boldsymbol{A}\boldsymbol{p}_i)\} \quad (A41)$$

$$(\boldsymbol{F}_{rr})_{i,k} = 2\mathrm{Re}\{(\boldsymbol{d}_{r_i}\tilde{\boldsymbol{\Pi}}_{\boldsymbol{A}}^{\perp}\boldsymbol{d}_{r_k})(\boldsymbol{p}_k^H \boldsymbol{A}^H \boldsymbol{R}^{-1}\boldsymbol{A}\boldsymbol{p}_i)\} \quad (A42)$$

Next, we consider the matrices $\boldsymbol{H}_\theta$ and $\boldsymbol{H}_r$. From (A22)–(A23) along with (A1), (A2), (A10), (A28), (A29), (A32), (A33), and (A39), the (i,k)th elements of $\boldsymbol{H}_\theta$ and $\boldsymbol{H}_r$ are given by

$$(\boldsymbol{H}_\theta)_{i,k} = 2\mathrm{Re}\{\tilde{\boldsymbol{e}}_m^T \boldsymbol{R}^{-1}\boldsymbol{A}\boldsymbol{p}_i\boldsymbol{d}_{\theta_k}^H\tilde{\boldsymbol{\Pi}}_{\boldsymbol{A}}^{\perp}\tilde{\boldsymbol{e}}_m\} \quad (A43)$$

$$(\boldsymbol{H}_r)_{i,k} = 2\mathrm{Re}\{\tilde{\boldsymbol{e}}_m^T \boldsymbol{R}^{-1}\boldsymbol{A}\boldsymbol{p}_i\boldsymbol{d}_{r_k}^H\tilde{\boldsymbol{\Pi}}_{\boldsymbol{A}}^{\perp}\tilde{\boldsymbol{e}}_m\} \quad (A44)$$

where the fact $d\boldsymbol{R}/d\sigma_m = d\boldsymbol{Q}/d\sigma_m = \tilde{\boldsymbol{e}}_m\tilde{\boldsymbol{e}}_m^T$ is used in (A43) and (A44).

At last, we consider the matrix $\boldsymbol{K}$ in (A18). By using (A1), (A2), (A10), (A30), (A31), and (A39), we can get the (i,k)th element of $\boldsymbol{K}$ as follows

$$(\boldsymbol{K})_{i,k} = 2\mathrm{Re}\{\tilde{\boldsymbol{e}}_m^T\tilde{\boldsymbol{\Pi}}_{\boldsymbol{A}}^{\perp}\tilde{\boldsymbol{e}}_m\tilde{\boldsymbol{e}}_m^T \boldsymbol{R}^{-1}\tilde{\boldsymbol{e}}_m\} - (\tilde{\boldsymbol{e}}_m^T\tilde{\boldsymbol{\Pi}}_{\boldsymbol{A}}^{\perp}\tilde{\boldsymbol{e}}_m)^2 \quad (A45)$$

Then, by performing some direct and tedious manipulations, we easily get

$$\boldsymbol{F}_{\theta\theta} = 2\mathrm{Re}\left\{(\tilde{\boldsymbol{D}}_\theta^H \boldsymbol{\Pi}_{\tilde{\boldsymbol{A}}}^{\perp}\tilde{\boldsymbol{D}}_\theta) \odot (\boldsymbol{R}_s\tilde{\boldsymbol{A}}^H\tilde{\boldsymbol{R}}^{-1}\tilde{\boldsymbol{A}}\boldsymbol{R}_s)^T\right\} \quad (A46)$$

$$\boldsymbol{F}_{\theta r} = 2\mathrm{Re}\left\{(\tilde{\boldsymbol{D}}_\theta^H \boldsymbol{\Pi}_{\tilde{\boldsymbol{A}}}^{\perp}\tilde{\boldsymbol{D}}_r) \odot (\boldsymbol{R}_s\tilde{\boldsymbol{A}}^H\tilde{\boldsymbol{R}}^{-1}\tilde{\boldsymbol{A}}\boldsymbol{R}_s)^T\right\} \quad (A47)$$

$$\boldsymbol{F}_{r\theta} = 2\mathrm{Re}\left\{(\tilde{\boldsymbol{D}}_r^H \boldsymbol{\Pi}_{\tilde{\boldsymbol{A}}}^{\perp}\tilde{\boldsymbol{D}}_\theta) \odot (\boldsymbol{R}_s\tilde{\boldsymbol{A}}^H\tilde{\boldsymbol{R}}^{-1}\tilde{\boldsymbol{A}}\boldsymbol{R}_s)^T\right\} \quad (A48)$$

$$\boldsymbol{F}_{rr} = 2\mathrm{Re}\left\{(\tilde{\boldsymbol{D}}_r^H \boldsymbol{\Pi}_{\tilde{\boldsymbol{A}}}^{\perp}\tilde{\boldsymbol{D}}_r) \odot (\boldsymbol{R}_s\tilde{\boldsymbol{A}}^H\tilde{\boldsymbol{R}}^{-1}\tilde{\boldsymbol{A}}\boldsymbol{R}_s)^T\right\} \quad (A49)$$

$$\boldsymbol{H}_\theta = 2\mathrm{Re}\left\{(\tilde{\boldsymbol{D}}_\theta^H \boldsymbol{\Pi}_{\tilde{\boldsymbol{A}}}^{\perp}) \odot (\tilde{\boldsymbol{R}}^{-1}\tilde{\boldsymbol{A}}\boldsymbol{R}_s)^T\right\} \quad (A50)$$

$$\boldsymbol{H}_r = 2\mathrm{Re}\left\{(\tilde{\boldsymbol{D}}_r^H \boldsymbol{\Pi}_{\tilde{\boldsymbol{A}}}^{\perp}) \odot (\tilde{\boldsymbol{R}}^{-1}\tilde{\boldsymbol{A}}\boldsymbol{R}_s)^T\right\} \quad (A51)$$

$$\boldsymbol{K} = 2\mathrm{Re}\left\{\boldsymbol{\Pi}_{\tilde{\boldsymbol{A}}}^{\perp} \odot \tilde{\boldsymbol{R}}^{-T}\right\} - \boldsymbol{\Pi}_{\tilde{\boldsymbol{A}}}^{\perp} \odot (\boldsymbol{\Pi}_{\tilde{\boldsymbol{A}}}^{\perp})^T \quad (A52)$$

where $\tilde{\boldsymbol{D}} = [\tilde{\boldsymbol{D}}_\theta, \tilde{\boldsymbol{D}}_r]$, $\tilde{\boldsymbol{D}}_\theta = \boldsymbol{Q}^{-1/2}\boldsymbol{D}_\theta$, $\tilde{\boldsymbol{D}}_r = \boldsymbol{Q}^{-1/2}\boldsymbol{D}_r$, $\boldsymbol{D}_\theta \triangleq [\boldsymbol{d}_{\theta_1}, \boldsymbol{d}_{\theta_2}, \ldots, \boldsymbol{d}_{\theta_K}]$, and $\boldsymbol{D}_r \triangleq [\boldsymbol{d}_{r_1}, \boldsymbol{d}_{r_2}, \ldots, \boldsymbol{d}_{r_K}]$.

Finally, by substituting (A46)–(A52) into (A15), we can establish $\mathrm{CRB}(\boldsymbol{\zeta})$ in (39) immediately. ∎

ACKNOWLEDGMENT

REFERENCES

[1] S. Haykin and A. Steinhardt, Eds, *Adaptive Radar Detection and Estimation.* New York, NY, USA: Wiley, 1992.

[2] D. H. Johnson and D. E. Dudgeon, *Array Signal Procsssing: Concepts and Techniques.* Englewood, NJ, USA: Prentice Hall, 1993.

[3] S. R. Saunders, *Antennas Propagatoin for Wireless Communication Systems.* Chichester, U.K.: Wiley, 1999.

[4] P. R. P. Hoole, Ed., *Smart Antennas and Signal Processing for Communications, Biomedical and Radar Systems.* Southampton, U.K.: WIT Press, 2001.

[5] H. L. Van Trees, *Optimum Array Processing, Part IV of Detection, Estimation, and Modulation Theory.* New York, NY, USA: Wiley, 2002.

[6] A. Bensky, *Wireless Positioning Techniques and Applications.* Morwood, MA, USA: Artech House, 2008.

[7] S. A. Zekavat and R. M. Buehrer, Eds, *Handbook of Position Location: Theory, Practice, and Advances*, 2nd Edition. Hoboken, NJ, USA: Wiley-IEEE Press, 2019.

[8] W. R. Hahn, "Optimum signal processing for passive sonar range and bearing estimation," *J. Acoust. Soc. Amer.*, vol. 58, vol. 1, pp. 201–207, 1975.

[9] S. Pasupathy and W. J. Alford, "Range and bearing estimation in passive sonar," *IEEE Trans. Aerosp. Electron. Syst.*, vol. AES-16, no. 2, pp. 244–249, 1980.

[10] Y. Rockah and P. Schultheiss, "Array shape calibration using sources in unknown locations–Part II: Near-field sources and estimator implementation," *IEEE Trans. Acoustics, Speech, Signal Process.*, vol. ASSP-35, no. 6, pp. 724–735, 1987.

[11] H. Krim and M. Viberg, "Two decades of array signal processing research: The parametric approach," *IEEE Signal Process. Mag.*, vol. 13, no. 4, pp. 67–94, Jul. 1996.

[12] A. Sahin and E. L. Miller, "Object detection using high resolution near-field array processing," *IEEE Trans. Geosci. Remote Sens.*, vol. 39, no. 1, pp. 136–141, Jan. 2001.

[13] C. Rascon and I. Meza, "Localization of sound sources in robotics: A review," *Robot. Auton. Syst.*, vol. 96, pp. 184–210, 2017.

[14] A. L. Swindlehurst and T. Kailath, "Passive direction-of-arrival and range estimation for near-field sources," in *Proc. IEEE 4th ASSP Workshop Spec. Est. Mod.*, Minneapolis, MN, USA, Aug. 3–5, 1988, pp. 123–128.

[15] Y. D. Huang and M. Barkat, "Near-field multiple source localization by passive sensor array," *IEEE Trans. Antennas Propagat.*, vol. 39, no. 7, pp. 968–975, Jul. 1991.

[16] A. J. Weiss and B. Friedlander, "Range and bearing estimation using polynomial rooting," *IEEE J. Oceanic Eng.*, vol. 18, no. 2, pp. 130–137, Apr. 1993.

[17] D. Starer and A. Nehorai, "Passive localization of near-field sources by path following," *IEEE Trans. Signal Process.*, vol. 42, no. 3, pp. 677–680, 1994.

[18] J. Lee, Y. Chen, and C. Yeh, "A covariance approximation method for near-field direction-finding using a uniform linear array," *IEEE Trans. Signal Process.*, vol. 43, no. 5, pp. 1293–1298, May 1995.

[19] J. Lee, C. Lee, and K. Lee, "A modified path-following algorithm using a known algebraic path," *IEEE Trans. Signal Process.*, vol. 47, no. 5, pp. 1407–1409, 1999.

[20] J. C. Chen, R. E. Hudson, and K. Yao, "Maximum-likelihood source localization and unknown sensor location estimation for wideband signals in the near-field," *IEEE Trans. Signal Process.*, vol. 50, no. 8, pp. 1843–1854, Aug. 2002.

[21] J. H. Lee and C. H. Tung, "Estimating the bearings of near-field cyclostationary signals," *IEEE Trans. Signal Process.*, vol. 50, no. 1, pp. 110–118, Jan. 2002.

[22] E. Boyer, A. Ferreol, and P. Larzabal, "Simple robust bearing-range source's localization with curved wavefronts," *IEEE Signal Process. Lett.*, vol. 12, no. 6, pp. 457–460, Jun. 2005.

[23] E. Grosicki, K. Abed-Meraim, and Y. Hua, "A weighted linear prediction method for near-field source localization," *IEEE Trans. Signal Process.*, vol. 53, no. 10, pp. 3651–3660, Oct. 2005.

[24] W. Zhi and M. Y. W. Chia, "Near-field source localization via symmetric subarrays," *IEEE Signal Process. Lett.*, vol. 14, no. 6, pp. 409–412, Jun. 2007.

[25] Y. S. Hsu, K. T. Wong, and L. Yeh, "Mismatch of near-field bearing-range spatial geometry in source–localization by a uniform linear array," *IEEE Trans. Antennas Propag.*, vol. 59, no. 10, pp. 3658–3667, Oct. 2011.

[26] L. Kumar and R. M. Hegde, "Near-field acoustic source localization and beamforming in spherical harmonics domain," *IEEE Trans. Signal Process.*, vol. 64, no. 13, pp. 3351–3361, Jul. 2016.

[27] P. Singh, Y. Wang, and P. Chargé, "A correction method for the near field approximated model based localization techniques," *Digital Signal Process.*, vol. 67, pp. 76–80, 2017.

[28] W. Zuo, J. Xin, N. Zheng, and A. Sano, "Subspace-based localization of far-field and near-field signals without eigendecomposition," *IEEE Trans. Signal Process.*, vol. 66, no. 17, pp. 4461–4476, Sep. 2018.

[29] W. Zuo, J. Xin, W. Liu, N. Zheng, H. Ohmori, and A. Sano, "Localization of near-field sources based on linear prediction and oblique projection operator," *IEEE Trans. Signal Process.*, vol. 67, no. 2, pp. 415–430, 2019.

[30] W. Zuo, J. Xin, H. Ohmori, N. Zheng, and A. Sano, "Subspace-based algorithms for localization and tracking of multiple near-field sources," *IEEE J. Sel. Topics Signal Process.*, vol. 13, no. 1, pp. 156–171, Mar. 2019.

[31] B. Friedlander, "Localization of signals in the near-field of an antenna array," *IEEE Trans. Signal Process.*, vol. 67, no. 15, pp. 3885–3893, 2019.

[32] V. Varanasi, A. Agarwal, and R.M. Hegde, "Near-field acoustic source localization using spherical harmonic features," *IEEE/ACM Trans. Audio, Speech, Language Process.*, vol. 27, no. 12, pp. 2054–2066, Dec. 2019.

[33] N. Yuen and B. Friedlander, "Performance analysis of higher order ESPRIT for localization of near-field sources," *IEEE Trans. Signal Process.*, vol. 46, no. 3, pp. 709–719, Mar. 1998.

[34] Y. Wu, L. Ma, C. Hou, G. Zhang, and J. Li, "Subspace-based method for joint range and DOA estimation of multiple near-field sources," *Signal Process.*, vol. 86, no. 8, pp. 2129–2133, 2006.

[35] G. Bienvenu, "Influence of the spatial coherence of the background noise on high resolution passive methods," in *Proc. IEEE Int. Conf. Acoust., Speech, Signal Process.*, Washington, DC, USA, Apr. 2-4, 1979, pp. 306–309.

[36] G. Bienvenu and L. Kopp, "Source power estimation method associated with high resolution bearing estimator," in *Proc. IEEE Int. Conf. Acoust., Speech, Signal Process.*, Atlanta, GA, USA, Mar. 30–Apr. 1, 1981, pp. 153–156.

[37] G. E. Martin, "Degradation of angular resolution for eigenvectoreigenvalue (EVEV) high resolution processors with inadequate estimation of noise coherence," in *Proc. IEEE Int. Conf. Acoust., Speech, Signal Process.*, San Diego, CA, USA, Mar. 19–21, 1984, pp. 758–761.

[38] A. Paulraj and T. Kailath, "Eigenstructure methods for direction of arrival estimation in the presence of unknown noise fields," *IEEE Trans. Acoust., Speech, Signal Process.*, vol. ASSP-34, no. 1, pp. 13–20, Feb. 1986.

[39] J. F. Bohme, "Estimation of spectral parameters of correlated signals in wavefields," *Signal Process.*, vol. 11, no. 4, pp. 329–337, 1986.

[40] S. Prasad, R. T. Williams, A. K. Mahalanabis, and L. H. Sibul, "A transform-based covariance differencing approach for some classes of parameter estimation problems," *IEEE Trans. Acoust., Speech, Signal Process.*, vol. 36, no. 5, pp. 631–641, May 1988.

[41] U. Nickel, "On the influence of channel errors on array signal processing methods," *Int. J. Electron. Comm.*, vol. 47, no. 4, pp. 209–219, 1993.

[42] B. Friedlander and A. J. Weiss, "On direction finding with unknown noise covariance," in *Proc. IEEE 28th Asilomar Conf. Signals Syst., Comput.*, vol. 2, Pacific Grove, CA, USA, Oct. 31–Nov. 2, 1994, pp. 780–784.

[43] V.F. Pisarenko, "The retrieval of harmonics from a covariance function," *Geophys. J. Roy. Astron. Soc.*, vol. 33, pp. 247–266, 1973.

[44] R. O. Schmidt, "Multiple emitter location and signal parameters estimation," in *Proc. RADC Spectrum Estimation Workshop*, Rome, NY, USA, Oct. 1979, pp. 243–258. Reprint in *IEEE Trans. Antennas Propag.*, vol. AP-34, no. 3, pp. 267–280, 1986.

[45] R. Kumaresan and D. W. Tufts, "Estimating the angles of arrival of multiple plane waves," *IEEE Trans. Aerosp. Electron. Syst.*, vol. AES-19, no. 1, pp. 134–139, Jan. 1983.

[46] R. Roy and T. Kailath, "ESPRIT–Estimation of signal parameters via rotational invariance techniques," *IEEE Trans. Acoust., Speech, Signal Process.*, vol. 37, no. 7, pp. 984–995, Jul. 1989.

[47] J. Xin and A. Sano, "Computationally efficient subspace-based method for direction-of-arrival estimation without eigendecomposition," *IEEE Trans. Signal Process.*, vol. 52, no. 4, pp. 876–893, Apr. 2004.

[48] J. P. Le Cadre, "Parametric methods for spatial signal processing in the presence of unknown colored noise fields," *IEEE Trans. Acoust., Speech, Signal Process.*, vol. 37, no. 7, pp. 965–983, Jul. 1989.

[49] P. Stoica, M. Viberg, and B. Ottersten, "Instrumental variable approach to array processing in spatially correlated noise fields," *IEEE Trans. Signal Process.*, vol. 42, no. 1, pp. 121–133, Jan. 1994.

[50] H. Ye and D. DeGroat, "Maximum likelihood DOA estimation and asymptotic Cramér-Rao bounds for additive unknown colored noise," *IEEE Trans. Signal Process.*, vol. 43, no. 4, pp. 938–949, 1995.

[51] V. Nagesha and S. Kay, "Maximum likelihood estimation for array processing in colored noise," *IEEE Trans. Signal Process.*, vol. 44, no. 2, pp. 169–180, Feb. 1996.

[52] M. Viberg, P. Stoica, and B. Ottersten, "Array processing in correlated noise fields based on instrumental variables and subspace fitting," *IEEE Trans. Signal Process.*, vol. 443, no. 5, pp. 1187–1199, May 1995.

[53] M. Viberg, P. Stoica, and B. Ottersten, "Maximum likelihood array processing in spatially correlated noise fields using parameterized signals," *IEEE Trans. Signal Process.*, vol. 45, no. 4, pp. 996–1004, Apr. 1997.

[54] W.-J. Zeng, X.-L. Li, and X.-D. Zhang, "Direction-of-arrival estimation based on the joint diagonalization structure of multiple fourth-order cumulant matrices," *IEEE Signal Process. Lett.*, vol. 16, no. 3, pp. 164–167, Mar. 2009.

[55] T. Li and A. Nehorai, "Maximum likelihood direction finding in spatially colored noise fields using sparse sensor arrays," *IEEE Trans. Signal Process.*, vol. 59, no. 3, pp. 1048–1062, 2011.

[56] A. B. Gershman, A. L. Matveyev, and J. F. Böhme, "Maximum likelihood estimation of signal power in sensor array in the presence of unknown noise field," *IEE Proc.–Radar, Sonar, Navig.*, vol. 142, no. 5, pp. 218–224, 1995.

[57] M. Pesavento and A.B. Gershman, "Maximum-likelihood direction-of-arrival estimation in the presence of unknown nonuniform noise," *IEEE Trans. Signal Process.*, vol. 49, no. 7, pp. 1310–1324, 2001.

[58] A. M. Zoubir and S. Aouada, "High resolution estimation of directions of arrival in nonuniform noise," in *Proc. IEEE Int. Conf. Acoust., Speech, Signal Process.*, vol. 2, Montreal, Canada, May 17–21, 2004, pp. 85–88.

[59] S. A. Vorobyov, A. B. Gershman, and K. M. Wong, "Maximum likelihood direction-of-arrival estimation in unknown noise fields using sparse sensor arrays," *IEEE Trans. Signal Process.*, vol. 53, no. 1, pp. 34–43, Jan. 2005.

[60] D. Madurasinghe, "A new DOA estimator in nonuniform noise," *IEEE Signal Process. Lett.*, vol. 12, no. 4, pp. 337–339, Apr. 2005.

[61] Y. Wu, C. Hou, G. Liao, and Q. Guo, "Direction-of-arrival estimation in the presence of unknown nonuniform noise fields," *IEEE J. Ocean. Eng.*, vol. 31, no. 2, pp. 504–510, Apr. 2006.

[62] C. Qi, Z. Chen, Y. Wang, and Y. Zhang, "DOA estimation for coherent sources in unknown nonuniform noise fields," *IEEE Trans. Aerosp. Electron. Syst.*, vol. 43, no. 3, pp. 1195–1204, Jul. 2007.

[63] C. E. Chen, F. Lorenzelli, R. E. Hudson, and K. Yao, "Stochastic maximum-likelihood DOA estimation in the presence of unknown nonuniform noise," *IEEE Trans. Signal Process.*, vol. 56, no. 7, pp. 3038–3044, Jul. 2008.

[64] L. Lu, H.-C. Wu, K. Yan, and S.S. Iyengar, "Robust expectation-maximization algorithm for multiple wideband acoustic source localization in the presence of nonuniform noise variances," *IEEE Sens. J.*, vol. 11, no. 3, pp. 536–544, 2011.

[65] A.-K. Seghouane, "A Kullback-Leibler methodology for unconditional ML DOA estimation in unknown nonuniform noise," *IEEE Trans. Aerosp. Electron. Syst.*, vol. 47, no. 4, pp. 3012–3021, Oct. 2011.

[66] B. Liao, S. Chan, L. Huang, and C. Guo, "Iterative methods for subspace and DOA estimation in nonuniform noise," *IEEE Trans. Signal Process.*, vol. 64, no. 12, pp. 3008–3020, Jun. 2016.

[67] B. Liao, L. Huang, C. Guo, and H. C. So, "New approaches to direction-of-arrival estimation with sensor arrays in unknown nonuniform noise," *IEEE Sensors J.*, vol. 16, no. 24, pp. 8982–8989, Dec. 2016.

[68] M. Esfandiari, S. A. Vorobyov, S. Alibani, and M. Karimi, "Non-iterative subspace-based DOA estimation in the presence of nonuniform noise," *IEEE Signal Process. Lett.*, vol. 26, no. 6, pp. 848–852, Jun. 2019.

[69] Q. Shen, H. Wan, and B. Liao, "A sparse representation based method for DOA estimation based in nonuniform noise," presented at the IEEE 23rd Int. Conf. Digital Signal Process., Shanghai, China, Nov. 19–21, 2018.

[70] Y. Zhu, X. Wang, L. Wan, M. Huang, W. Feng, and J. Wang, "Unitary low-rank matrix decomposition for DOA estimation in nonuniform noise," presented at the IEEE 23rd Int. Conf. Digital Signal Process., Shanghai, China, Nov. 19–21, 2018.

[71] Y. Wang, X. Yang, J. Xie, L. Wang, and B.W.-H. Ng, "Sparsity-inducing DOA estimation of coherent signals under the coexistence of mutual coupling and nonuniform noise," *IEEE Access*, vol. 7, pp. 40271–40278, 2019.

[72] W. Tan and X. Feng, "Covariance matrix reconstruction for direction finding with nested arrays using iterative reweighted nuclear norm minimization," *Int. J. Antennas Propag.*, vol. 2019, 2019, Art. no. 7657898.

[73] X. Wang, Y. Zhu, M. Huang, J. Wang, L. Wan, and G. Bi, "Unitary matrix completion-based DOA estimation of noncircular signals in nonuniform noise," *IEEE Access*, vol. 7, pp. 73719–73728, 2019.

[74] H. Wang, L. Wan, M. Dong, K. Ota, and X. Wang, "Assistant vehicle localization based on three collaborative base stations via SBL-based robust DOA estimation," *IEEE Int. Things J.*, vol. 6, no. 3, pp. 5766–5777, 2019.

[75] G. Jiang, M. Wang, X. Mao, C. Qian, Y. Liu, and A. Nehorai, "Underdetermined direction-of-arrival estimation using difference coarray in the presence of unknown nonuniform noise," *IEEE Access*, vol. 7, pp. 157643–15654, 2019.

[76] N. Guzey, H. Xu, and S. Jagannathan, "Localization of near-field sources in spatially colored noise," *IEEE Trans. Instrum. Meas.*, vol. 64, no. 8, pp. 2302–2311, Aug. 2015.

[77] K. Wang, L. Wang, J.-R. Shang, and X.-X. Qu, "Mixed near-field and far-field source localization based on uniform linear array partition," *IEEE Sensors J.*, vol. 16, no. 22, pp. 8083–8090, Nov. 2016.

[78] J. Song, H. Tao, J. Xie, and C. Sun, "Mixed far-field and near-field source localization algorithm via sparse subarrays," *Int. J. Antennas Propag.*, vol. 2018, Art. no. 3237167, 2018.

[79] K. Wang, L. Wang, Z. Zhang, and J. Xie, "Algebraic algorithm for mixed near-field and far-field sources classification and localization," *Prog. Electromagn. Res.*, vol. 83, pp. 125–136, 2018.

[80] A. M. Molaei, B. Zakeri, and S. M. H. Andargoli, "Passive localization and classification of mixed near-field and far-field sources based on high-order differencing algorithm," *Signal Process.*, vol. 157, pp. 119–130, 2019.

[81] A. M Molaei, A. Ramezani-Varkani, and M. R. Soheilifar, "A pure cumulant-based method with low computational complexity for classification and localization of multiple near and far field sources using a symmetric array," *Prog. Electromagn. Res.*, vol. 96, pp. 123–138, 2019.

[82] A. M. Molaei, B. Zakeri, and S. M. H. Andargoli, "Components separation algorithm for localization and classification of mixed near-field and far-field sources in multipath propagation," *IEEE Trans. Signal Process.*, vol. 68, pp. 404–419, 2020.

[83] A. M. Molaei, B. Zakeri, and S. M. H. Andargoli, "High-performance localization of mixed fourth-order stationary sources based on a spatial/temporal full ESPRIT-like method," *Signal Process.*, vol. 171, Art. 107468, 2020.

[84] J. Qing, C. Jin-fang, and X. Da-wei, "Research on high-order cumulant ESPRIT algorithm based on single AVS," in *Proc. 1st Int. Conf. Electr. Instru. Inf. Systems*, Harbin, China, Jun. 3–5, 2017.

[85] W. Zuo, J. Xin, N. Zheng, and A. Sano, "Subspace-based localization of near-field signals in unknown nonuniform noise," in *Proc. IEEE 10th Sensor Array Multichannel Signal Process. Workshop*, pp. 247–251, Sheffield, UK, Jul. 8–11, 2018.

[86] R. T. Behrens and L. L Scharf, "Signal processing applications of oblique projection operators," *IEEE Trans. Signal Process.*, vol. 42, no. 6, pp. 1413-1424, Jun. 1994.

[87] H. C. So, "Source localization: Algorthim and analysis," in *Proc. Handbook of Position Location: Theory, Practice, Advances*, 2nd Ed. Hoboken, NJ: Wiley-IEEE Press, 2019.

[88] K. C. Ho and M. Sun, "Passive sources ocalization using time differences of arrival and gain rtatios of arrival," *IEEE Trans. Signal Process.*, vol. 56, no. 2, pp. 464–477, Feb. 2008.

[89] Y. Wang and K.C. Ho, "TDOA positioning irrespective of source range," *IEEE Trans. Signal Process.*, vol. 65, no. 6, pp. 1447–1460, Mar. 2017.

[90] Y. Sun, K. C. Ho, and Q. Wan, "Solution and analysis of TDOA localization of a near or distant source in closed form," *IEEE Trans. Signal Process.*, vol. 67, no. 2, pp. 320–335, Jan. 2019.

[91] H. Tao, J. Xin, J. Wang, N. Zheng, and A. Sano, "Two-dimensional direction estimation for a mixture of noncoherent and coherent signals," *IEEE Trans. Signal Process.*, vol. 63, no. 2, pp. 318–333, Jan. 2015.

[92] W. Liu, W. Zuo, J. Xin, N. Zheng, and A. Sano, "Localization of near-field signals based on linear prediction and oblique projection operator," in *Proc. 26th Europ. Sig. Process. Conf.*, pp. 341–345, Rome, Italy, Sep. 3–7, 2018.

[93] W. Zuo, J. Xin, N. Zheng, and A. Sano, "New subspace-based method for localization of multiple near-field signals and statistical analysis," in *Proc. IEEE 52nd Asilomar Conf. Signals, Systems, Computers*, pp. 1152–1156, Pacific Grove, CA, Oct. 28–31, 2018.

[94] J. Xie, H. Tao, X. Rao, and J. Su, "Comments on 'Near-field source localization via symmetric subarrays,'" *IEEE Signal Process. Lett.*, vol. 22, no. 5, pp. 643 644, May 2015.

[95] P. Stoica and A. Nehorai, "MUSIC, maximum likelihood, and Cramer-Rao bound," *IEEE Trans. Acoust., Speech, Signal Process.*, vol. 37, no. 5, pp. 720–741, May 1989.

[96] M. N. El Korso, R. Boyer, A. Renaux, and S. Marcos, "Conditional and unconditional Cramér-Rao bounds for near-field source localization," *IEEE Trans. Signal Process.*, vol. 58, no. 5, pp. 2901–2907, 2010.

[97] Y. Begriche, M. Thameri, and K. Abed-Meraim, "Exact Cramer Rao bound for near field source localization," in *Proc. 11th Int. Conf. Inf. Sci., Signal Process. Appl.*, pp. 718–721, Montreal, Canada, Jul. 2–5, 2012.

[98] J. P. Delmas and H. Gazzah, "CRB analysis of near-field source localization using uniform circular arrays," in *Proc. IEEE Int. Conf. Acoust., Speech, Signal Process.*, pp. 3996–4000, Vancouver, Canada, May 26–31, 2013.

[99] H. Gazzah and J. P. Delmas, "CRB-based design of linear antenna arrays for near-field source localization," *IEEE Trans. Antennas Propagat.*, vol. 62, no. 4, pp. 1965–1974, 2014.

[100] A. B. Gershman, M. Pesavento, P. Stoica, and E. G. Larsson, "The stochastic CRB for array processing in unknown noise fields," in *Proc. IEEE Int. Conf. Acoust., Speech, Signal Process.*, pp. 2989–2992, vol. 5, Salt Lake City, UT, May 7–11, 2001.

[101] A. B. Gershman, P. Stoica, M. Pesavento, and E. G. Larsson, "Stochastic Cramér–Rao bound for direction estimation in unknown noise fields," *IEE Proc.-Radar Sonar Nav.*, vol. 149, no. 1, pp. 2–8, 2002.

[102] P. Stoica, E. G. Larsson, and A. B. Gershman, "The stochastic CRB for array processing: A textbook derivation," *IEEE Signal Process. Lett.*, vol. 8, no. 5, pp. 148–150, May 2001.

[103] G. H. Golub and C. F. Van Loan, *Matrix Computations*, 2nd Ed. Baltimore, MD: John Hopkins Univ. Press, 1989.

[104] A. Graham, *Kronecker Products Matrix Calculus with Applications*. New York: Wiley, 1981.

[105] M. Malek-Mohammadi, M. Jansson, A. Owrang, A. Koochakzadeh, and M. Babaie-Zadeh, "DOA estimation in partially correlated noise using low-rank/sparse matrix decomposition," in *Proc. IEEE 8th Sensor Array, Multichannel Signal Process. Workshop*, pp. 373–376, A Coruna, Spain, Jun. 22–25, 2014.

[106] B. Liao, C. Guo, L. Huang, and J. Wen, "Matrix completion based direction-of-arrival estimation in nonuniform noise," in *Proc. IEEE Int. Conf. Digital Signal Process.*, pp. 66–69, Beijing, China, Oct. 16–18, 2016.

[107] B. Liao, C. Guo, and H. C. So, "Direction-of-arrival estimation in nonuniform noise via low-rank matrix decomposition," in *Proc. 22nd Int. Conf. Digital Signal Process.*, London, U.K., Aug. 23–25, 2017.

[108] M. Wax, "Detection and localization of multiple sources in noise with unknown covariance," *IEEE Trans. Signal Process.*, vol. 40, no. 1, pp. 245–249, Jan. 1992.

[109] K. M. Wong, J. P. Reilly, Q. Wu, and S. Qiao, "Estimation of the directions of arrival of signals in unknown correlated noise, Part I: The MAP approach and its implementation," *IEEE Trans. Signal Process.*, vol. 40, no. 8, pp. 2007–2017, Aug. 1992.

[110] Q. Wu, K. M. Wong, and J. P. Reilly, "Maximum likelihood direction-finding in unknown noise environments," *IEEE Trans. Signal Process.*, vol. 42, no. 4, pp. 980–983, Apr. 1994.

[111] B. Friedlander and A. J. Weiss, "Direction finding using noise covariance modeling," *IEEE Trans. Signal Process.*, vol. 43, no. 7, pp. 1557–1567, Jul. 1995.

[112] B. Goransson and B. Ottersten, "Direction estimation in partially unknown noise fields," *IEEE Trans. Signal Process.*, vol. 47, no. 9, pp. 2375–2385, Sep. 1999.

[113] M. Agrawal and S. Prasad, "A modified likelihood function approach to DOA estimation in the presence of unknown spatially correlated Gaussian noise using a uniform linear array," *IEEE Trans. Signal Process.*, vol. 48, no. 10, pp. 2743–2749, Oct. 2000.

[114] N. Tayem, H. M. Kwon, S. Min, and D. H. Kang, "Covariance matrix differencing for coherent source DOA estimation under unknown noise field," in *Proc. IEEE 64th Veh. Technol. Conf.*, Montral, Canada, Sep. 25–28, 2006.

Weiliang Zuo (Member, IEEE) received the B.E. degree in electrical engineering and the Ph.D. degree in control science and engineering, from Xi'an Jiaotong University, Xi'an, China, in 2010 and 2018, respectively.

During 2016 to 2017, he was a visiting Ph.D. student in the School of Electrical and Computer Engineering at Georgia Institute of Technology (Georgia Tech). He is currently an Assistant Professor in the College of Artificial Intelligence, Xi'an Jiaotong University. His current research interests include array and statistical signal processing, pattern recognition, and medical imaging processing.

Jingmin Xin (Senior Member, IEEE) received the B.E. degree in information and control engineering from Xi'an Jiaotong University, Xi'an, China, in 1988, and the M.S. and Ph.D. degrees in electrical engineering from Keio University, Yokohama, Japan, in 1993 and 1996, respectively.

From 1988 to 1990, he was with the Tenth Institute of Ministry of Posts and Telecommunications (MPT) of China, Xi'an. He was with the Communications Research Laboratory, Japan, as an Invited Research Fellow of the Telecommunications Advancement Organization of Japan (TAO) from 1996 to 1997 and as a Postdoctoral Fellow of the Japan Science and Technology Corporation (JST) from 1997 to 1999. He was also a Guest (Senior) Researcher with YRP Mobile Telecommunications Key Technology Research Laboratories Company, Limited, Yokosuka, Japan, from 1999 to 2001. From 2002 to 2007, he was with Fujitsu Laboratories Limited, Yokosuka, Japan. Since 2007, he has been a Professor at Xi'an Jiaotong University. His research interests are in the areas of adaptive filtering, statistical and array signal processing, system identification, and pattern recognition.

Nanning Zheng (Fellow, IEEE) graduated from the Department of Electrical Engineering, Xi'an Jiaotong University, Xi'an, China, in 1975, and received the M.S. degree in information and control engineering from Xi'an Jiaotong University in 1981 and the Ph.D. degree in electrical engineering from Keio University, Yokohama, Japan, in 1985.

He joined Xi'an Jiaotong University in 1975, and is currently a Professor and the Director of the Institute of Artificial Intelligence and Robotics, Xi'an Jiaotong University. His research interests include computer vision, pattern recognition and image processing, and hardware implementation of intelligent systems.

Dr. Zheng became a member of the Chinese Academy of Engineering in 1999, and he is the Chinese Representative on the Governing Board of the International Association for Pattern Recognition. He also serves as an Executive Deputy Editor of the Chinese Science Bulletin.

Hiromitsu Ohmori (Member, IEEE) received the B.E., M.E., and Ph.D. degrees in electrical engineering from Keio University, Yokohama, Japan, in 1983, 1985 and 1988, respectively. In April 1988, he became an Instructor with the Department of Electrical Engineering, Keio University, where he became an Assistant Professor in April 1991. In April 1996, he became an Associate Professor with the Department of System Design Engineering, Keio University, where he is currently a Professor. In April 2020, he became a Guest Professor of Hiroshima University. His research interests are in the field of adaptive control, robust control, nonlinear control, and their applications. He is member of the SICE, ISCIE, IEE, IEICE, and EICA.

Akira Sano (Member, IEEE) received the B.E., M.S., and Ph.D. degrees in mathematical engineering and information physics from the University of Tokyo, Japan, in 1966, 1968, and 1971, respectively.

In 1971, he joined the Department of Electrical Engineering, Keio University, Yokohama, Japan, where he was a Professor with the Department of System Design Engineering till 2009. He is currently Professor Emeritus of Keio University. He has been a member of Science Council of Japan since 2005. He was a Visiting Research Fellow at the University of Salford, Salford, U.K., from 1977 to 1978. He is the coauthor of the textbook *State Variable Methods in Automatic Control* (Wiley, 1988). His current research interests are in adaptive modeling and design theory in control, signal processing and communication, and applications to control of sounds and vibrations, mechanical systems, and mobile communication systems.

Dr. Sano is a Fellow of the Society of Instrument and Control Engineers and is a Member of the Institute of Electrical Engineering of Japan and the Institute of Electronics, Information and Communications Engineers of Japan. He was General Co-Chair of 1999 IEEE Conference of Control Applications and an IPC Chair of 2004 IFAC Workshop on Adaptation and Learning in Control and Signal Processing. He was the Chair of IFAC Technical Committee on Modeling and Control of Environmental Systems from 1996 to 2001. He has also been Vice Chair of IFAC Technical Committee on Adaptive Control and Learning since 1999 and the Chair of IFAC Technical Committee on Adaptive and Learning Systems since 2002. He was also on the Editorial Board of Signal Processing. He was the recipient of the Kelvin Premium from the Institute of Electrical Engineering in 1986.